J. Fluid Mech. (2005), *vol.* 526, *pp.* 303–336.
DOI: 10.1017/S0022112004003088 Printed in the United Kingdom

Combined effects of favourable pressure gradient and streamline curvature on uniformly sheared turbulence

By A. G. L. HOLLOWAY, D. C. ROACH AND H. AKBARY

Department of Mechanical Engineering, University of New Brunswick,
PO Box 4400 Fredericton, NB Canada E3B 5A3
holloway@unb.ca

(Received 3 November 2003 and in revised form 20 October 2004)

The combined effects of favourable pressure gradient and streamline curvature were studied experimentally using an approximately homogeneous uniformly sheared turbulence. The shear flow was initially generated in a straight wind tunnel, where the turbulence was allowed to develop a fixed stress anisotropy, and then subsequently directed into a curved wind-tunnel test section. Streamwise pressure gradients were applied by convergence of the curved tunnel walls in the plane of the mean shear. In one set of experiments, convergence was applied in the first half of the curved test section, but not in the second half. In another set of experiments, the convergence was applied in the second half of the curved test section, but not in the first. This arrangement permitted the study of application and removal of streamwise pressure gradient to curved shear flow. Measurements showing the response of the turbulence stresses to the changing mean strain rates are reported and are consistent with previous studies which show that stabilizing curvature diminishes the turbulence energy and stresses. The addition of the streamwise strain rate associated with favourable pressure gradient was observed to have the effect of further diminishing the turbulence activity and its overall anisotropy. However, the important shear component of the anisotropy was increased above what it would be under the influence of curvature alone. The removal of streamwise strain rate caused the turbulence to recover a structure similar to that measured for uniformly curved shear flow; although this adjustment included an increase in the shear component of anisotropy prior to its gradual relaxation.

The principal direction of the Reynolds stress tensor was found to be closely related to the principal direction of the mean strain rate tensor in the present flows. This result was also found to be valid in the outer layer of accelerating curved boundary layers. A relationship between the direction of the principal mean strain rate and the mean flow curvature and streamwise strain rate was formulated to explain how each influences the state of turbulence stress.

1. Introduction

Turbulent shear layers in the form of boundary layers, wakes, mixing layers, jets and various combinations of these, arise frequently in technological and natural flows. They are critical regions of momentum and heat transport for which the character of the turbulence is highly influential. This turbulence evolves subject to external constraints imposed by solid and irrotational flow boundaries. In many practical

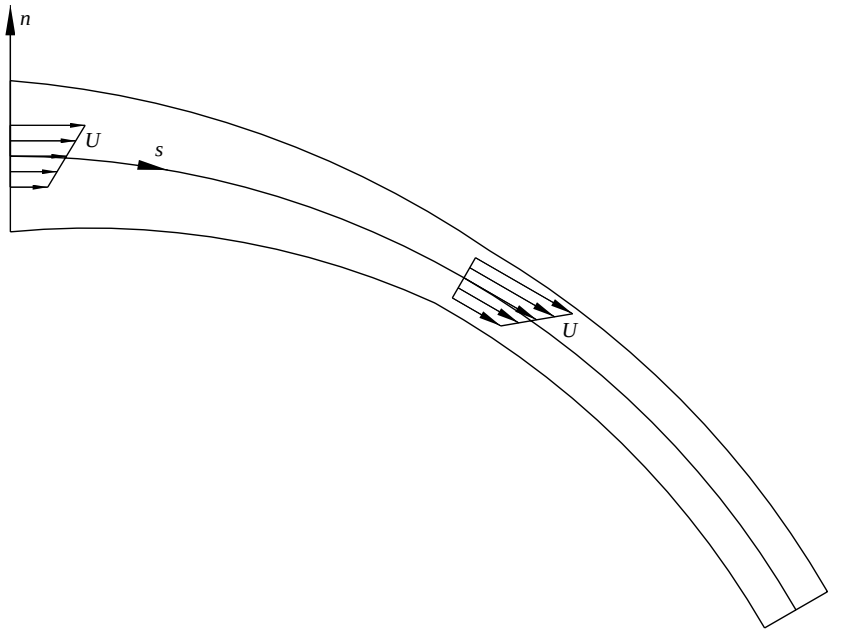

FIGURE 1. Schematic drawing of accelerating curved shear flow showing the curvilinear coordinates used for its description.

circumstances, these external conditions include streamwise pressure gradients and curvature. This is especially true of boundary layers where external flow curvature is essential for the production of the pressure gradients. Specifically, lifting aerofoils have boundary layers that are predominantly convex and experience strong favourable and weak adverse pressure gradients. Highly cambered aerofoils, such as those used in turbo-machinery, may also include significant regions of concave curvature. Both pressure gradient and surface curvature have been shown to have a significant effect on boundary-layer turbulence; although traditional boundary-layer analysis has regarded streamwise pressure gradient as more important.

In the context of boundary layers, flow curvature is directly related to centripetal acceleration, $\rho U_e^2/R$, and therefore to the radial pressure gradient in the external flow, where R is the local radius of surface curvature, U_e is the speed of the external flow, and ρ is the fluid density. Similarly, the streamwise pressure gradient may be equated to streamwise acceleration, $-\rho U_e \mathrm{d}U_e/\mathrm{d}s$, where s is the distance along the surface. The curvature and streamwise strain rates imposed on the outer edge of the boundary layer can be deduced from these acceleration components and their ratio is exactly equal to the ratio of the strain rates, $(\mathrm{d}U_e/\mathrm{d}s)/(U_e/R)$. This ratio is approximately constant across a thin shear layer. In typical aerofoil applications, both streamwise and normal components of acceleration are of similar orders of magnitude over most of the surface with all four quadrants in the plane of acceleration occupied. The present study considers only flows having favourable pressure gradient and convex curvature.

The objective of the present work was to study the combined effects of favourable pressure gradient and streamwise curvature on sheared turbulence using a simplified flow in which the mean shear, flow curvature and mean streamwise strain rate were approximately uniform and direct wall and entrainment effects were absent (see figure 1). Such a flow is an extension of the homogeneous shear-flow problem that has been the subject of extensive theoretical, numerical and experimental studies.

Previous experimental studies of uniformly sheared turbulence, including curvature, are included in the data bank AGARD AR-345 (1998) for the purposes of testing LES and other models of turbulence. The value of this class of flows lies in the simplicity of their boundary conditions and statistical description combined with the inclusion of the essential elements of turbulence production and energy redistribution. The present accelerating, curved, shear flow was developed in stages with the uniform shear flow generated in a straight wind-tunnel section and the flow curvature generated by guiding the flow into a wind tunnel of constant centreline curvature. The streamwise pressure gradient is applied by convergence of the curved wind-tunnel walls in the plane of the shear. In all cases, the tunnel walls converge at a constant rate which, it will be shown in a later section, produces a fixed value of $(\partial U/\partial s)/U^2$. The turbulence of this flow remains approximately homogeneous on transverse planes within the central core of the tunnel and the turbulence development under the influence of the uniform mean strains is measured along the windtunnel centreline. In this flow, the streamline convergence is coincident with mean flow acceleration (favourable pressure gradient) and mean streamwise strain rate. Throughout this paper, reference will be made to all four terms; however, it is the mean streamwise strain rate that best correlates the observed effects on the turbulence.

2. Literature review

There exists a substantial amount of literature on the effects of streamline curvature on shear-layer turbulence. The early literature was reviewed by Bradshaw (1973) in the context of curvature being an 'extra strain' imposed on the shear layer. This approach also considered streamwise strain resulting from flow acceleration as an 'extra strain'. It was identified that turbulent shear-layer development is much more sensitive to curvature than laminar shear layers (or their stability). This sensitivity to curvature cannot be explained by the explicit curvature terms in the Reynolds stress transport equations. Generally it has been observed that convex surface curvature diminishes boundary-layer turbulence levels and concave surface curvature enhances turbulence levels, compared to uncurved flow. The sensitivity of a sheared turbulence to convex curvature is generally reported to be greater. This result has been generalized to other shear layer types by recognizing that the boundary layer on a convex surface has a mean velocity increasing outward from the centre of curvature while the concave boundary layer has the mean velocity decreasing outward from the centre of curvature; convex and concave curvature are referred to as positive and negative curvature, respectively. These observed changes in turbulence activity are accompanied by changes in mixing length. A gross measure of the strength of curvature effects is δ/R, where δ is the shear-layer thickness and R is the mean radius of curvature of the shear layer with $\delta/R < 0.05$, indicating mild effects, and $\delta/R > 0.1$, strong effects. Another measure of curvature introduced in the early literature and reviewed by Bradshaw (1973) is the ratio of curvature-imposed strain to the mean shear rate. Expressed in curvilinear coordinates running along the shear layer, this takes the form $S = (U/R)/(\partial U/\partial n)$, where U/R is the strain rate produced by curvature and $\partial U/\partial n$ is the mean shear rate. We can interpret S in other ways; for example, it is the ratio of production (negative) of turbulence kinetic energy due to curvature strain to the production due to shear strain; a Richardson number, based on an analogy between curvature-induced body forces and buoyancy; and a ratio of turbulence to extra strain rate time scales, using the inverse shear rate as a measure of the turbulence time scale. One of the conclusions reached by Bradshaw (1973) was that

the changes in turbulence shear stress due to prolonged application of extra strain rate could be modelled by $\overline{uv}/\overline{uv}_0 = (1 - 10S)$. A similar conclusion for the application of streamwise strain rate $\overline{uv}/\overline{uv}_0 = (1 - 4Q)$ where $Q = (\partial U/\partial s)/(\partial U/\partial n)$ was also proposed. In the case of changing curvature, the adjustment length of boundary-layer-turbulence was taken to be 10δ.

Many excellent experimental studies of curvature have been performed during the 30 years following Bradshaw (1973). These include both positive (convex) and negative (concave) curvature of jets, wakes, mixing layers, duct flows and boundary layers. Many of these were designed with considerable care to eliminate extraneous effects such as streamwise pressure gradient. Boundary-layer and duct flows were reviewed by Bandyopdhyay (1989) and Patel & Sotiropoulos (1997). Studies of curved mixing layers have been published by Castro & Bradshaw (1976) and Plesniak, Mehta & Johnston (1994) and studies of curved wakes by Savill (1983), Ramjee & Neelakandan (1989), Weygandt & Mehta (1995) and Koyama (1981, 1983). These experiments served to reinforce the early work by adding many details to the broad view described above. They also provide test cases for turbulence model calibration. One of the results that may be derived from these studies is that convex curvature produces a loss of anisotropy of the large-scale turbulence motions of which the shear stress is only one measure. In contrast, concave surface curvature enhances the anisotropy of the large-scale motions. There is no perceptible effect of curvature on the small-scale motions of turbulence. In spite of this large body of experimental work, Patel & Sotiropoulos (1997) conclude that little insight into how streamwise flow curvature affects the turbulence has been achieved.

A simple curved flow having a uniform shear and a nearly homogeneous turbulence was introduced by Holloway & Tavoularis (1992, hereinafter referred to as HT). This study is directly relevant to the present work since it includes a curved test section where the sheared turbulence was exposed to prolonged constant curvature. A wide range of curvature effects was explored using different tunnel curvatures and mean shear rates. This study was designed to reveal the direct effect of curvature on sheared turbulence by eliminating the complicating effects of flow inhomogeneity, intermittency and pressure gradients. Of course, it does not provide information about the effects of curvature on turbulent diffusion or the near-wall layers. The study covered an experimental range $-0.5 < S < 1.0$. The turbulence of the more strongly sheared flows (low $|S|$) developed a fixed structure, and exponent of growth, within the tunnel test section that was well correlated with S. For example, the dimensionless shear stress, $\overline{uv}/q^2$ (where q^2 is twice the turbulence kinetic energy per unit mass) is a sensitive measure of curvature effects, and was found to follow the rule $\overline{uv}/q^2 = -0.14(1 - 3.0S)\mathrm{sgn}(S)$ in the range $-0.2 < S < 0.3$. The change in sign for $S > 0.33$, which produced counter-gradient momentum transport, was observed. The turbulence stresses and integral length scales were found to grow exponentially for $S < 0.05$ and decay for $S > 0.05$. Subsequent experiments of uniformly curved shear flow included Chebbi, Holloway & Tavoularis (1998) where curvature was reversed within an S-shaped tunnel to reveal the response of uniformly sheared turbulence to changing curvature. The experiment considered the curvature sequence: $S = 0.0, +0.05, -0.05, 0.$ and $S = 0, -0.05, +0.05, 0.$ It was found that the equilibrium structure observed by HT was approached in each subsection after approximately 4.5 units of shear strain. The initial adjustment being proportional to the angle of curvature, and the relaxation distance being proportional to the inverse shear rate. Chebbi *et al.* (1998) also examined some of the curved boundary-layer data and showed that the uniformly curved shear-flow results were consistent with what had been observed

in the outer region of boundary layers when one accounts for the local shear rate. In particular, insight as to the sensitivity of the outer boundary-layer turbulence to convex turbulence, the edge of the so-called 'active shear stress layer' (Gillis & Johnston 1983) and the adjustment length for changes in curvature was provided.

Modelling of curvature effects has progressed from correlating the changes in mixing length, or eddy viscosity, that accompany streamline curvature to transport models based on the explicit flow curvature effects in the production and advection terms of the Reynolds stress equations. Patel & Sotiropoulos (1997) describe these in some detail as they apply to boundary-layer flows and conclude that each level of model may be made to fit the data satisfactorily with tuning of the model constants, although none is completely satisfactory. A model parameter of particular interest to the present study is the rate of change of the principal mean strain rate direction, $\mathrm{d}\theta/\mathrm{d}t$, introduced by Spalart & Shur (1997) as a measure of curvature and rotation effects and a replacement for U/R. This variable is directly applicable to homogeneous curved flows and its applicability to flows with pressure gradient will be explored. An explanation of curvature effects that was based on the inherent rotation of the shear direction with respect to inertial coordinates that accompanies curved flows was presented by Holloway & Tavoularis (1998). It provided semi-analytical expressions for the Reynolds stress anisotropy measured in the experiment of HT for the prolonged application of constant curvature. It was also demonstrated in the paper that a number of popular Reynolds stress transport models do not model the Reynolds stress anisotropy that develops under prolonged streamline curvature accurately. The arguments in Holloway & Tavoularis (1998) have since been extended by Holloway & Roach (2001) to predict the anisotropy of the integral length scales.

The effects of favourable pressure gradient on boundary-layer turbulence are important because of their role in flow stability and skin friction. Streamwise pressure gradients can be generated by lateral convergence of the flow, transverse plane convergence, or a combination of the two. In the present study, we will concern ourselves only with the plane, or two-dimensional, convergence case. An early literature review on accelerating boundary-layer studies, in the absence of curvature, was provided by Narishima & Sreenivasen (1973) with an interest towards boundary-layer relaminarization. Experimental studies of accelerating boundary layers have been published by Blackwelder & Kovasznay (1972), Spalart & Watmuff (1993), Fernholz & Warnack (1998) and Warnack & Fernholz (1998). Gross measures of pressure gradient effects on boundary layers are $(\delta/\tau_w)(\mathrm{d}P_e/\mathrm{d}x)$ or $(\nu/U_e^3)(\mathrm{d}P_e/\mathrm{d}x)$. Blackwelder & Kovasznay (1972) and Warnack & Fernholz (1998) report that, for $(\nu/U_e^3)(\mathrm{d}P_e/\mathrm{d}x) \sim 4 \times 10^{-6}$, the near-wall turbulence activity is suppressed, the viscous layer thickens, and the skin friction coefficient is increased. This inner-layer effect scales with viscosity, and therefore is not included in the present experimental study. (Note that $Q = 0$ on the surface.) In the outer regions of the boundary layer, the normal components of the Reynolds stresses approach one another, while the shear stress and the turbulence kinetic energy remain practically unaffected in spite of a diminished mean shear. Warnack & Fernolz (1998) showed that $\overline{uv}/q^2$ increased by 25% as a result of the streamwise acceleration. The finding pertinent to the present work, although perhaps not the most significant for this class of flow, is the behaviour of the outer layer; but neither of the above measures of pressure gradient is directly related to the extra strain rate parameter, $Q = (\partial U/\partial s)/(\partial U/\partial n)$. It was established using the mean velocity profiles presented by that Balckwelder & Kovasnay (1972) that $Q_{max} \sim 0.35$ at a boundary-layer location of $y/\delta \sim 0.5$. Similarly, Case 1 of Fernholz &

Warnack (1998) has $Q_{max} \sim 0.17$. Both of these studies will be discussed further in § 7.2.

There have been a considerable number of studies on the combined effects of streamwise curvature and pressure gradient on shear-layer turbulence in recent years. Published studies include accelerating boundary layers on curved surfaces, wake flows and uniform shear flows. The boundary-layer studies appear in three forms: (i) flow on a uniformly curved surface with pressure gradient (Schwarz, Plesniak & Murthy 2002); (ii) boundary-layer flow over a surface with a two-dimensional bump (Wu & Squires 1998; Webster, DeGraaff & Eaton 1996; Baskaran, Smits & Joubert 1987, 1991); and (iii) boundary-layer development in an S-shaped duct (Bandyopadhyay & Ahmed 1993; Lopes & Piomelli 2003). A curved wake flow with favourable pressure gradient has been studied by Nakayama (1987). Each of these studies reports more or less detailed turbulence measurements and, in particular, the structural parameter, $\overline{uv}/q^2$, which was found to be sensitive to both curvature and streamwise acceleration. Some also provide insightful, albeit incomplete, analysis of curvature and acceleration effects using the Reynolds stress equations. Unfortunately, the strain history of some of these flows is very complex, such as the flow over a hill and the curved duct flow, and a quantitative comparison of the observed effects to the present flow would require the use of a comprehensive model which is beyond the scope of the present study.

The study by Schwarz *et al.* (2002) is the simplest of the flows listed above and presents a strain history very similar to the present work and will be used for comparison to the present results. It considered a constant, convex surface curvature combined with favourable and adverse pressure gradients. The purpose was to investigate the effect of combining strains due to curvature and pressure gradient on the boundary-layer turbulence. Conditions of moderate and strong curvature ($\delta/R > 0.05$ and 0.10, respectively) were considered in combination with moderate and strong favourable pressure gradient, with $10^6(\nu/U_e^3)(\mathrm{d}P_e/\mathrm{d}x) = 0.5$ and 1.0. Note that the pressure gradient is not strong enough to cause relaminarization in the absence of curvature. Schwarz *et al.* (2002) introduced the ratio of streamwise and radial pressure gradients, $P_{rat} = (\partial P/\partial s)/(\partial P/\partial n) = (-U_e\,\mathrm{d}U_e/\mathrm{d}s)/(U_e^2/R)$, which is exactly equal to $-Q/S$ (defined above) throughout the boundary layer. Considered separately, S and Q are exactly zero on the surface and maximum at the outer edge; both S and Q decline with increasing flow Reynolds number owing to the increased shear rate in the boundary layer. Schwarz *et al.* (2002) present combinations of strong curvature with moderate and strong pressure gradient giving $Q/S = 1.2$ and 0.6. The angles turned within the measurement sections were 30° and 55° for the 0.7 m radius wall and 0.4 m radius walls, respectively. Profiles of mean velocity, turbulence stresses in the plane of curvature, principal angle of the Reynolds stress tensor, and total shear strain parameter (Maxey 1982) are reported for various streamwise positions. The authors draw a number of conclusions, including the following. (i) The inner part of the wall layer ($y^+ < 50$) can be scaled in terms of inner-layer variables for all cases considered. (ii) The outer layer is strongly affected by combined curvature and streamwise acceleration. The effect, stronger in the $Q/S = 1.2$ case, is to reduce the turbulence velocities and their correlation. (iii) Convex curvature reduces the principal angle of the Reynolds stress (moves it towards the streamwise direction) and favourable pressure gradient counteracts this reduction. (iv) Favourable pressure gradient increases the total strain substantially.

An experimental study of the effects of favourable pressure gradient on curved uniform shear flows was conducted by Akbary (1997). It was a predecessor of the

experiments of Roach (2001) and, in fact, used an earlier version of the same experimental facility. The flow configurations covered by Akbary were simultaneous application of streamwise pressure gradient and curvature and simultaneous removal of streamwise pressure gradient and curvature. The experiments spanned a range of $-0.2 < S < +0.2$ and $0 < Q < 0.3$ with the cases of strongest curvature and streamwise strain rate corresponding to the mild cases of the present flow. A significant difference between these flows and those of the present study is that the present study used a straight tunnel of twice the length providing more development distance before the application of curvature. Two of the flows of Akbary (1997) that are complementary to the present results will be reviewed in the discussion section.

To summarize, laboratory studies of the combined effects of streamwise curvature and favourable pressure gradient on turbulence exist for wakes, boundary layers and duct flows within a rather limited range of flow conditions. There is agreement among these studies, at least in the qualitative sense, on the general effects on the turbulence; for example, both convex curvature and favourable pressure gradient reduce the turbulence activity and cause adjustments in the structural parameter, $\overline{uv}/q^2$. Furthermore, in their own context, each flow is a valuable contribution that may be regarded quantitatively. However, the unique features of each flow make it difficult to compare the detailed effects among flows and thereby develop the type of generalization that is an important feature of insightful turbulence modelling. For example, an important and outstanding question is whether the effects of curvature and favourable pressure gradient on turbulence may be regarded as independent and therefore additive. This is a difficult question to answer with generality based on say, boundary-layer turbulence, because of the interaction of the wall boundary condition and favourable pressure gradient that is absent from wake flow. In fact, these extraneous features are difficult to model accurately in their own right and this can greatly increase the uncertainty of interpretation. There is then a need for an experimental study of a turbulent shear flow having both flow curvature and favourable pressure gradient and as few other extraneous features as possible so that it may represent a common element of all of the flows listed above. At present, a study of this type does not exist in the literature and the flow described here is an attempt to address this deficiency. The measurements presented describe the development of an initially sheared turbulence in a mean flow that may be idealized for the purposes of computation as a homogeneous field of strain that includes elements of shear, curvature and streamwise acceleration.

3. Analytical considerations

3.1. *Description of the flow*

The subject of the present study is a curved, converging flow with uniform shear. A schematic of an accelerating curved shear flow can be seen in figure 1. Because of the nature of the geometry, a curvilinear coordinate system that runs parallel to the mean streamlines is best to describe the flow (Bradshaw 1973). The origin of which is set at the start of the curvature, with $s = 0$, and on the flow centreline, $n = z = 0$. The centreline radius is denoted by R_c. The three components of velocity are tangent to the s, n and z coordinate directions, respectively. The components, of mean velocity will be denoted by U, V and W and the components of the velocity fluctuation by u, v and w. Angles in the (s, n)-plane are measured as positive in the counterclockwise direction.

3.2. *A model of the mean flow*

An aerodynamic analysis of the uniform shear flow illustrated in figure 1 is given to provide insight into the effects of curvature and streamwise acceleration on the mean velocity profile. For this purpose, we first restrict our analysis to the core of the wind tunnel and exclude the boundary layers and associated non-uniformities. Throughout the wind-tunnel test sections, the flow is assumed to be two-dimensional with vorticity components, $\zeta_s = \zeta_n = 0$ and ζ_z a constant, equal to its value in the straight tunnel section in which the shear was generated. (It should be noted that in the core of the wind tunnel, the direct viscous action is negligible and that the net turbulent diffusion is exactly zero for homogeneous turbulence.) The volume flow rate per unit depth, f, is also conserved so that the values of streamfunction are constant on the upper and lower boundaries. The vorticity in this flow is defined as

$$\zeta_z = \left(1 + \frac{n}{R_c}\right)^{-1} \left(\frac{\partial V}{\partial s} - \frac{U}{R_c}\right) - \frac{\partial U}{\partial n}, \tag{1}$$

that for the present analysis we will reduce to the expression,

$$\zeta_z = -\left(1 + \frac{n}{R_c}\right)^{-1} \frac{U}{R_c} - \frac{\partial U}{\partial n}, \tag{2}$$

valid in regions where $\partial V/\partial s$ is small or, in other words, between sections having sudden changes in radius, R_c, or tunnel height, h. Integrating (2) gives a circumferential velocity of Couette form composed of irrotational and rotational parts,

$$U = \frac{A}{n + R_c} + B(n + R_c), \tag{3}$$

where A depends on the local values of h and R_c

$$A = \frac{2(q - h\zeta_z R_c)}{\ln((h + R_c)/(R_c - h))} \tag{4}$$

and $B = \varsigma_z/2$. The streamfunction for the flow can be derived from (3) using the definition $U = \partial\psi/\partial n$ as

$$\psi = A \ln\left(\frac{n + R_c}{R_c - h}\right) + B(n^2 - h^2) + B R_c(n + h), \tag{5}$$

with $\psi = 0$ on the lower flow boundary ($n < 0$). Total pressure is conserved along lines of constant streamfunction so that the static pressure may be determined from Bernoulli's equation.

The radial profiles of velocity and pressure that result from (3) and Bernoulli's equation applied along streamlines are shown in figure 2 for the initial straight tunnel with nominal values: $U_c = 10\,\mathrm{m\,s^{-1}}$, $\zeta_z = \partial U/\partial n = 27\,\mathrm{s^{-1}}$, a curved tunnel of $R_c = 3\,\mathrm{m}$ and curved tunnels of equal curvature after various degrees of flow convergence. The uniform profiles of velocity generated in the straight wind tunnel change only slightly as a result of applying curvature, and the effects of flow convergence tend to return the profile to a linear form. The pressure in the initial straight tunnel is uniform, after curvature it has adjusted by rising at the outer wall and falling at the inner wall. The streamline that enters on the centreline of the curved tunnel migrates to smaller radii, but there is little pressure gradient in this region. With flow convergence the pressure decreases, more so at the inner surface.

A relationship between centreline velocity and channel height may, for the practical purposes at hand, be based on the near linearity of the velocity profiles. This leads to

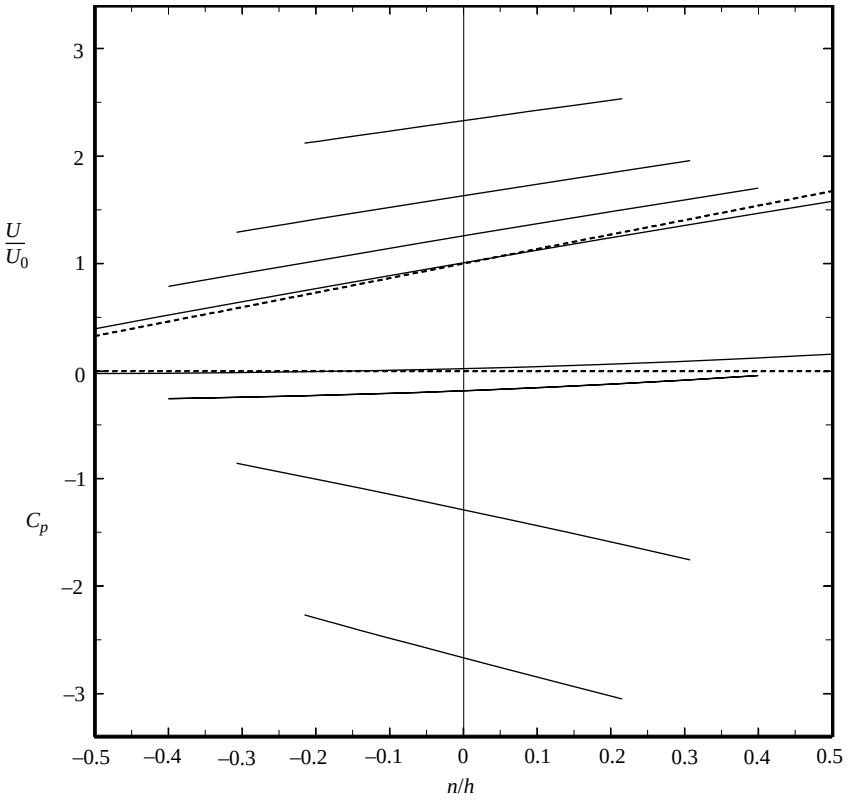

FIGURE 2. Development of velocity and pressure profiles of an initially uniform shear flow subjected to flow curvature and convergence. Results are based on an inviscid model of uniform vorticity and fixed two-dimensional flowrate. Line length indicates the degree of flow convergence. The dashed lines indicate profiles in the initial straight flow.

the approximate relationship, $f = U_c h$, and therefore

$$\frac{1}{U_c^2}\frac{\mathrm{d}U_c}{\mathrm{d}s} = -\frac{1}{f}\frac{\mathrm{d}h}{\mathrm{d}s}. \tag{6}$$

In the present experiments, the rate of flow convergence, $\mathrm{d}h/\mathrm{d}s$, was fixed and we see that (6) implies that the streamwise strain rate, $\mathrm{d}U_c/\mathrm{d}s$, increases along the tunnel as does the streamwise acceleration, $U_c \mathrm{d}U_c/\mathrm{d}s = -\partial P/\partial s$.

We now consider the strain rate field of the curved converging flow. The mean strain rate on the tunnel centerline ($n = 0$) for $V = 0$ has the tensor form

$$\boldsymbol{d} = \tfrac{1}{2}\begin{pmatrix} 2\dfrac{\partial U}{\partial s} & \dfrac{\partial U}{\partial n} - \dfrac{U}{R} \\ \dfrac{\partial U}{\partial n} - \dfrac{U}{R} & -2\dfrac{\partial U}{\partial s} \end{pmatrix}, \tag{7}$$

with $d_{11} = -d_{22}$ for mean flow continuity. The principal strain rates in the (s, n)-plane are

$$d_{1,2} = \pm\tfrac{1}{2}\sqrt{\left(2\frac{\partial U}{\partial s}\right)^2 + \left(\frac{\partial U}{\partial n} - \frac{U}{R}\right)^2}, \tag{8}$$

with the first principal strain rate, d_1, inclined to the s-coordinate at the angle

$$\theta = \tfrac{1}{2}\tan^{-1}\left(\frac{\dfrac{\partial U}{\partial n} - \dfrac{U}{R}}{2\dfrac{\partial U}{\partial s}}\right) = \tfrac{1}{2}\tan^{-1}\left(\frac{1-S}{2Q}\right) \tag{9}$$

and d_2 at 90° to d_1. The direction of pure shear in this flow is at the angle $\beta = \theta - 45°$ and the maximum shear rate is numerically equal to the principal strain rate.

Equations (8) and (9) show that both streamwise strain and curvature affect the principal strain rates and directions of the principal axes. In the case of a fixed streamwise strain rate, the direction of the principal axes, or equivalently the direction of maximum shear, is fixed relative to the s-coordinate direction and ranges from 45° for $Q = 0$ to 0° for large Q. However, a changing streamwise strain rate causes the principal axes to rotate relative to the s-coordinate direction at the rate

$$\frac{\mathrm{d}\theta}{\mathrm{d}s} = \frac{-Q\dfrac{\partial S}{\partial s} - (1-S)\dfrac{\partial Q}{\partial s}}{(1-S)^2 + 4Q^2}. \tag{10}$$

Equation (10) is consistent with the general formula given by Spalart & Shur (1997) for rate of rotation of principal mean strain rate axes. An increasing streamwise strain rate intensifies the principal rate of strain and diminishes the rate of rotation of the strain rate axes relative to the (s, n)-coordinates.

Curvature alone, whether constant or not, has no effect on the angle of principal strain rate relative to the s-coordinate direction. However, in a curved flow, the direction tangent to coordinate s, when viewed from a frame convected at the mean speed, U_c, is itself rotating relative to the laboratory frame at the rate $\Omega = -U_c/R_c$. Therefore, the application of flow curvature causes a rotation of the direction of the principle strain rate, or direction of maximum shear, relative to fixed laboratory coordinates. The vorticity relative to this rotating frame of reference becomes

$$\zeta_z^I = -\left(\frac{U}{R_c} + \frac{\partial U}{\partial n}\right) - 2\Omega = -\left(\frac{\partial U}{\partial n} - \frac{U}{R_c}\right), \tag{11}$$

which is exactly equal to the rate of shear strain in the absence of streamwise strain. In other words, the mean strain field of a non-accelerating uniformly curved flow viewed in a frame convected at the mean speed can be interpreted as a rotating parallel shear flow. We can see then that both curvature and streamwise strain rate affect the angle of principal mean strain rate when measured relative to an inertial frame. This analysis is, of course, limited to the immediate vicinity of the tunnel centreline where the mean strains may be considered approximately homogeneous and there is no solid boundary that would fix the streamline direction relative to the laboratory frame.

4. Turbulence

4.1. *Reynolds stresses*

The components of the Reynolds stress per unit mass expressed in (s, n)-coordinates are: $\overline{u^2}$, $\overline{v^2}$, $\overline{w^2}$, $\overline{uv}$, $\overline{uw}$, and $\overline{vw}$ with the latter two shear components identically zero in the present flow, owing to the plane symmetry. The sum of the normal stresses, $q^2 = \overline{u^2} + \overline{v^2} + \overline{w^2}$, is twice the kinetic energy of the turbulence per unit mass and is invariant to rotation of the coordinate axes.

The principal stresses in the (s, n)-plane are

$$\sigma_{1,2} = \frac{\overline{u^2} + \overline{v^2}}{2} \pm \sqrt{\left(\frac{\overline{u^2} - \overline{v^2}}{2}\right)^2 + \overline{uv}^2}, \tag{12}$$

with the inclination of the principal stress axes to the s-coordinate given by

$$\gamma = \tfrac{1}{2}\tan^{-1}\left(\frac{2\overline{uv}}{\overline{u^2} - \overline{v^2}}\right). \tag{13}$$

For uncurved non-accelerating uniform shear flow with $\partial U/\partial n > 0$, $\gamma \sim -20^\circ$ to the streamwise direction. The plane of maximum shear stress, $\beta = \gamma - 45^\circ$.

The deviation of the Reynolds stress tensor from isotropic form can be evaluated by the components of the dimensionless anisotropy tensor $m_{ij} = \overline{u_i u_j}/q^2 - \delta_{ij}/3$, where $u_i = (u, v, w)$ and δ_{ij} is the unit tensor. In the present flows prior to the start of curvature and acceleration ($\partial U/\partial n > 0$), the anisotropy of the turbulence is

$$m_{ij} = \begin{pmatrix} 0.20 \pm 0.02 & -0.15 \pm 0.02 & 0 \\ -0.15 \pm 0.02 & -0.15 \pm 0.01 & 0 \\ 0 & 0 & -0.06 \pm 0.01 \end{pmatrix}. \tag{14}$$

Previous studies of uniformly sheared turbulence (HT) have shown similar anisotropy of the turbulence.

The equations describing the development of the Reynolds stresses along the tunnel centreline ($n = 0$) are (Nakayama 1987; Baskaran *et al.* 1991)

$$\frac{\mathrm{D}}{\mathrm{D}t}\left(\tfrac{1}{2}\overline{u^2}\right) = -\left(\overline{u^2}\frac{\partial U}{\partial s} + \overline{uv}\left(\frac{\partial U}{\partial n} + \frac{U}{R_c}\right)\right) + \phi_{uu} - \varepsilon_{uu}, \tag{15}$$

$$\frac{\mathrm{D}}{\mathrm{D}t}\left(\tfrac{1}{2}\overline{v^2}\right) = \left(\overline{v^2}\frac{\partial U}{\partial s} + 2\overline{uv}\frac{U}{R_c}\right) + \phi_{vv} - \varepsilon_{vv}, \tag{16}$$

$$\frac{\mathrm{D}}{\mathrm{D}t}\left(\tfrac{1}{2}\overline{w^2}\right) = \phi_{ww} - \varepsilon_{ww}, \tag{17}$$

$$\frac{\mathrm{D}}{\mathrm{D}t}\overline{uv} = -\overline{v^2}\left(\frac{\partial U}{\partial n} - \frac{U}{R}\right) + 2(\overline{u^2} - \overline{v^2})\frac{U}{R_c} + \phi_{uv} - \varepsilon_{uv}, \tag{18}$$

where $\mathrm{D}()/\mathrm{D}t$ is the mean convective derivative along the tunnel centreline ($n = 0$). ϕ represents the pressure–strain-rate correlation and ε the viscous destruction. The remaining terms result from the effects of mean strain and rotation on the stress tensor. Neither the mean pressure gradient, nor the mean acceleration, appear explicitly in (15) to (18), only the mean strain rates.

We can see that streamwise strain rate reduces $\overline{u^2}$ and increases $\overline{v^2}$, but has no effect on the correlation $\overline{uv}$. The absolute mean vorticity increases $\overline{u^2}$, and the frame rotation decreases $\overline{v^2}$. The mean strain rate and frame rotation affect the correlation $\overline{uv}$.

The equation governing the development of $\overline{q^2}$ along the centreline of the tunnel is

$$\frac{\mathrm{D}q^2}{\mathrm{D}t} = -2(\overline{u^2} - \overline{v^2})\frac{\partial U}{\partial s} - 2\overline{uv}\left(\frac{\partial U}{\partial n} - \frac{U}{R_c}\right) + \phi_{q^2} - \varepsilon_{q^2}. \tag{19}$$

For anisotropic turbulence with $\overline{u^2} > \overline{v^2}$ and $\overline{uv} < 0$, the streamwise strain rate and curvature reduce q^2 while the shear increases it.

The effects of curvature and streamwise strain based on the explicit mean strain rates appearing in (15)–(19) will be shown to be qualitatively consistent with the present measurements. However, these direct effects of the mean strain rates are mitigated by the turbulent action of the small scales and the pressure–strain-rate correlation and these two terms must be accurately modelled before quantitative predictions are possible.

4.2. *Scales of development*

In simple homogeneous shear flow the only scale imposed by the mean flow is the shear rate (Harris, Graham & Corrsin 1977) and the stresses and length scales grow with the total mean shear strain $\tau = \int_{t_o}^{t} (\partial U/\partial n)\,\mathrm{d}t$, where, moving with the mean centreline speed, $\mathrm{d}t = \mathrm{d}s/U_c$.

In the case of curved shear flow, there are two time scales imposed by the mean velocity field, $\partial U/\partial n$ and U/R_c (HT). It was shown by Chebbi *et al.* (1998) that, immediately following a change of flow curvature, the development of the turbulence scales according to the angle, $\theta = -\int_{s_o}^{s} (U/R_c)\,\mathrm{d}t$ and then increasingly with the mean shear strain, $\tau = \int_{t_o}^{t} (\partial U/\partial n - U/R_c)\,\mathrm{d}t$, until the components of turbulence anisotropy and exponents of growth approach fixed values that depend only on the ratio, S. This transition is complete by $\tau = 4.5$.

In the present flow, there are three time scales imposed by the mean field; $\partial U/\partial n$, U/R_c, and $\partial U/\partial s$. Based on the above findings, we might expect that in the converging curved shear flow, which is the subject of the present study, the mean shear would still determine the period of adjustment to changes in the mean field and may still be used to scale the exponents of growth of the turbulence scales, but that these exponents, and the equilibrium values of anisotropy, would depend on both S and Q.

5. Experimental apparatus and instrumentation

5.1. *The wind-tunnel facility*

The wind tunnel at the University of New Brunswick is of the open-return type shown in figure 3. This type of wind tunnel is the most practical for the generation, development and manipulation of uniform shear flows and has been used in several previous studies. It is equipped with a mixed flow fan and a 20 h.p. variable speed d.c. motor. The flow is conditioned with a large settling chamber and a 16:1 contraction that produces a flow non-uniformity of less than 1% and a turbulence intensity of $< 0.1\%$ at the exit of the nozzle.

A uniform shear flow is produced using a shear generator placed immediately downwind of the nozzle. It had 23 separate parallel channels each with an adjustable flow resistance to produce a velocity profile that varied nearly linearly across the core of the test section. In practice, the resistance of each channel must be tuned to obtain the linear variation of the mean flow. The shear generator was followed by a 0.4 m long 'flow developer' (Karnik & Tavoularis 1987) with 23 obstruction-free channels aligned with those of the shear generator. It was used to make the length scales of the turbulence leaving the shear generator more uniform in the transverse direction by allowing them to develop briefly in these restrictive channels of equal height. The shear generator also serves to couple the mean shear rate to the mean speed on the tunnel centreline, so that $(\partial U/\partial n)/U_c =$ constant, and as a consequence

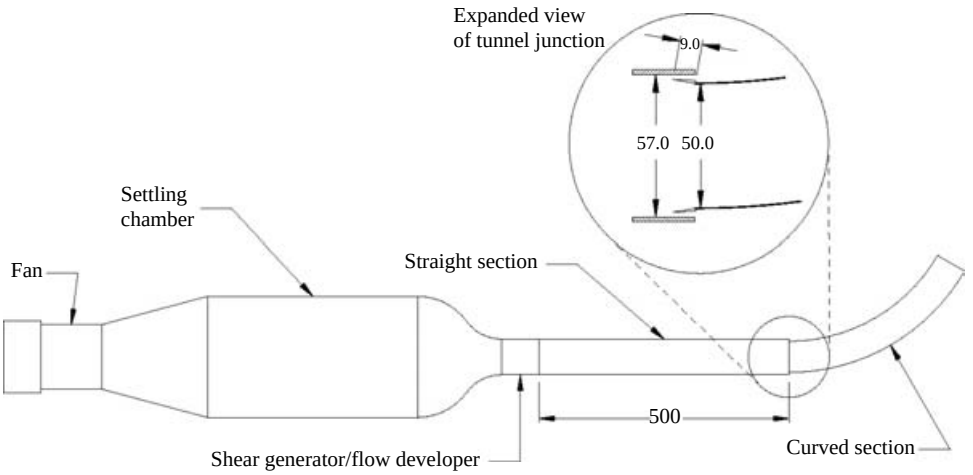

FIGURE 3. Schematic of wind tunnel showing straight and curved tunnel test sections. The junction between the straight and curved wind-tunnel test is similar in plan view. All dimensions are in cm.

the turbulence stresses scale with the centreline mean speed in the laboratory frame (Karnik & Tavoularis 1987).

The straight tunnel test section was 5 m in length and located directly downwind of the flow developer. The straight tunnel allows the turbulence to homogenize and to develop an asymptotic state under the influence of uniform shearing as described by Tavoularis & Karnik (1989); thus providing a well-defined initial state of the turbulence for the subsequent application of flow curvature and streamwise acceleration. The cross-sectional dimensions of the straight tunnel were nominally 57 cm $\times$ 57 cm, though the sidewalls could be manipulated over the last half of the section to compensate for boundary-layer growth.

Once the flow reached the end of the straight section, it passed tangentially into the curved portion of the wind tunnel which had a centreline radius of 3 m and a streamwise extent of 314 cm. The sidewalls of the curved section were made from Plexiglas^{TM} with slots cut for the insertion of probes into the airflow. The upper and lower walls were made from rolled aluminium sheets and in two sections to allow for the sequential application of different strains. Figure 4 shows the dimensions of the curved test section.

The curved tunnel was made with a smaller cross-section than the straight tunnel (50 cm $\times$ 50 cm) to permit the removal of the boundary layers which had developed along the straight tunnel walls. The junction between the straight and curved test sections is shown in figure 3. The flaps along the upper and lower surfaces of the curved tunnel entrance were adjusted to help guide the flow through the transition and maintain continuity of the mean speed and turbulence statistics. Along the curved test section, a small amount of flow was removed from the corners to prevent boundary-layer separation. As a consequence, the flow is only approximately conserved along the length of the curved tunnel.

The probe was positioned in the curved tunnel along the 3 coordinate axes via a computer and a Centroid CNC-3 stepper motor controller. This controller was capable of positioning the probe to within 0.1 mm in the n- and z-directions and to within 1 mm in the streamwise direction. These accuracies were considered sufficient

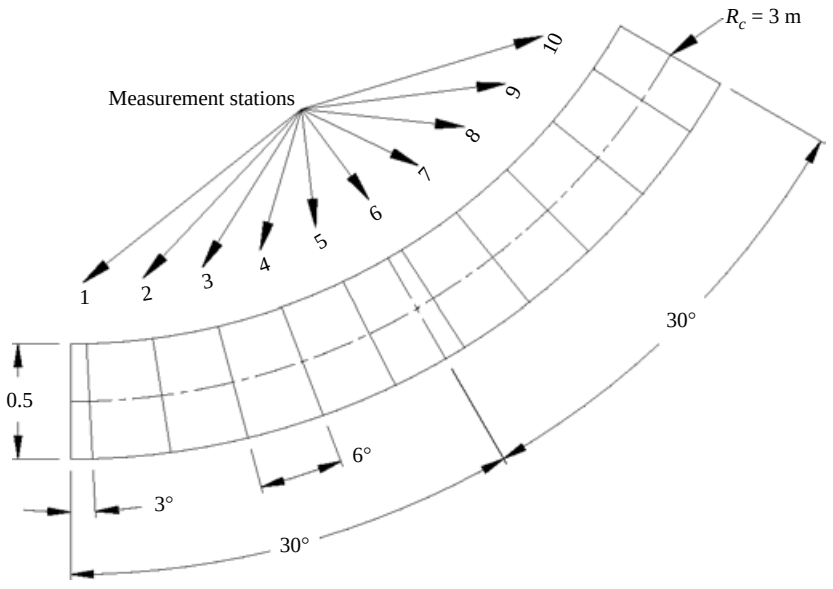

Station	s (cm)
1	2.8
2	34.2
3	65.6
4	97.0
5	128.4
6	159.8
7	191.2
8	222.7
9	254.1
10	280.0

FIGURE 4. Curved wind-tunnel test section showing overall dimensions and measurement stations. The first and second sections may be converged independently to develop the flow convergence. There is no flow convergence in the configuration shown.

because of the weak spatial inhomogeneity of the flow. Measurements were taken in each of several (n, z)-planes. The locations of these points varied among experiments and from plane to plane depending on the flow development. Once all of the desired planes were completed, streamwise measurements along the centreline were taken in the straight and curved sections of the tunnel. Measurements in the curved section were limited to the first 280 cm owing to a deterioration of flow quality near the end of the tunnel.

5.2. *Instrumentation and measurement uncertainty*

The fluid velocity was measured using standard constant temperature hot-wire anemometry techniques (Bruun 1995). A Dantec P61 X-wire probe in conjunction with two Dantec 56C17 anemometers were used to measure two components of the fluid velocity simultaneously. The sensing elements are made from 5 μm diameter tungsten wire, were 1.25 mm long and separated by 0.9 mm. All streamwise integral scales measured in the present flows were larger than 50 mm and therefore it may be concluded that the effects of wire size on the energy-containing scales of the flow are negligible.

Directional calibration of the hot wires for pitch consisted of fitting an effective wire angle to the cosine cooling law as described by Bradshaw (1972). The yaw angle was less than 12°, 95 % of the time in the turbulence and therefore the out-of-plane velocity was not considered as it contributed less than 1 % of the wire cooling. Speed calibration of the hot wires was performed in the wind tunnel under laminar flow conditions with the probe placed at the first measurement point. The data were fitted using least-squares to a modified form of King's law which accounted for changes in mean air temperature that were measured continuously by a thermistor immersed in the air flow (Roach 2001).

Variable	Value	Uncertainty	Value	Uncertainty
U ($\mathrm{m\,s^{-1}}$)	9.78	1.3%	21.99	1.1%
V ($\mathrm{m\,s^{-1}}$)	0.46	0.20 $\mathrm{m\,s^{-1}}$	0.368	0.45 $\mathrm{m\,s^{-1}}$
W ($\mathrm{m\,s^{-1}}$)	0.02	0.20 $\mathrm{m\,s^{-1}}$	−0.414	0.45 $\mathrm{m\,s^{-1}}$
q^2 ($\mathrm{m\,s^{-2}}$)	0.642	3.7%	0.621	3.5%
m_{uu}	0.200	0.011	0.080	0.011
m_{vv}	−0.151	0.010	−0.049	0.010
m_{ww}	−0.049	0.010	−0.030	0.009
m_{uv}	−0.139	0.009	−0.125	0.008

TABLE 1. Uncertainties in turbulence statistics for high and low speeds. Values correspond to a 95% confidence interval.

The voltage signals from the anemometer bridges were low-pass filtered at 10 kHz with a 6-pole Butterworth filter to remove electronic noise and then offset and amplified so that the signals were in an appropriate range for digitization. The data were sampled with a Keithley Metrabyte DAS-20 analogue to digital converter (ADC) with a SSH-4 simultaneous sample and hold. The ADC had a resolution of 12 bits and was set to a range of ± 0.5 V (giving ± 0.12 mV as the least significant bit). Sampling was done at 2 kHz to produce record lengths of 4096 points. This sampling rate and record length were experimentally determined to be sufficient for the calculation of the mean velocity and Reynolds stresses for the present flow conditions. Fifty pairs of 4096 points were taken at each measurement point to provide a statistical basis. Once all the measurement points had been visited, the probe was rotated about its axis by 90° and the process repeated to measure the third component of the velocity.

The velocity statistics were derived from the evenly spaced discrete velocity samples by simple arithmetic averaging. An uncertainty analysis was performed using the method of Chebbi *et al.* (1998) and the results are given in table 1 for two speed ranges, corresponding to the unaccelerated and accelerated flows. They include both systematic and statistical errors.

6. Measurements

6.1. *Experimental conditions*

Two levels of tunnel wall convergence were tested with two sequences of the curvature and streamwise strain, for a total of four experiments. All flows started with uncurved shear flow in which the components of the stress anisotropy had developed stable values before the start of the curved test section (see (14)). In two of the flows, the strain sequence consisted of the application of curvature alone in the first curved subsection followed by the application of flow convergence in the second curved subsection. These flows were denoted as A_m or A_s depending on the strength of flow convergence applied. In the other two flows, curvature and flow convergence were applied simultaneously in the first curved subsection followed by the removal of convergence in the second curved subsection. These flows were denoted by R_m or R_s. Schematics of the tunnel configurations used to produce these flows are shown in figure 5 and a summary of flow conditions is shown in table 2.

The amount of data collected in a given (n, z)-plane was determined by the distance between the upper and lower walls; as the tunnel walls converged, fewer points were

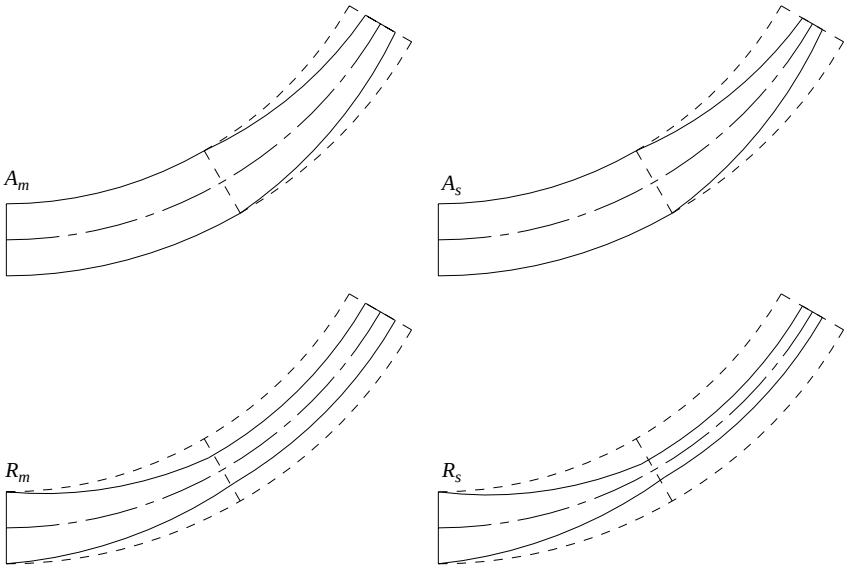

FIGURE 5. The four converged flow configurations used for the present study. Configurations A_m and A_s apply flow convergence to a curved shear flow. Configurations R_m and R_s remove flow convergence from a curved shear flow. Tunnel centreline, along which development of turbulence is measured, has a constant radius of curvature of 3 m in all configurations. Outer dashed lines show undeflected wall positions.

Flow	Prior to the start of curvature $s < 0$	First curved subsection $0 < s < 157$ cm	Second curved subsection 15 cm $< s <$ 314 cm
A_m	$U_c = 9.9\ \mathrm{m\,s^{-1}}$ $\partial U/\partial n = 25\ \mathrm{s^{-1}}$	Curvature alone: $R_c = 3$ m, $h_i = 0.5$ m, $h_f = 0.5$ m	Curvature with convergence: $R_c = 3$ m, $h_i = 0.5$ m, $h_f = 0.24$ m
A_s	$U_c = 9.9\ \mathrm{m\,s^{-1}}$ $\partial U/\partial n = 29\ \mathrm{s^{-1}}$	Curvature alone: $R_c = 3$ m, $h_i = 0.5$ m, $h_f = 0.5$ m	Curvature with convergence: $R_c = 3$ m, $h_i = 0.5$ m, $h_f = 0.16$ m
R_m	$U_c = 9.7\ \mathrm{m\,s^{-1}}$ $\partial U/\partial n = 25\ \mathrm{s^{-1}}$	Curvature with convergence: $R_c = 3$ m, $h_i = 0.5$ m, $h_f = 0.24$ m	Curvature alone: $R_c = 3$ m, $h_i = 0.24$ m, $h_f = 0.24$ m
R_s	$U_c = 10.3\ \mathrm{m\,s^{-1}}$ $\partial U/\partial n = 29\ \mathrm{s^{-1}}$	Curvature with convergence: $R_c = 3$ m, $h_i = 0.5$ m, $h_f = 0.16$ m	Curvature alone: $R_c = 3$ m, $h_i = 0.16$ m, $h_f = 0.16$ m

TABLE 2. Details of the flow configurations studied. Tunnel width was 50 cm.

measured. It ranged from 244 points to 124 points arranged in a two-dimensional array. For the first level of convergence, the distance between the tunnel walls was reduced to 24 cm, while for the stronger case, it was reduced to 16 cm. These represent nominal cross-sectional area reductions of 52% and 68%, respectively. The speed up of the centreline flow was less in all cases owing to air bled from the corners and the adjustment of the streamlines resulting from the imposition of curvature.

6.2. *Mean flow*

The development of the normalized mean circumferential velocity along the centreline of the curved test section for all four flows is shown in figure 6. The streamwise location of measurement stations in figure 4 are indicated at the top of the graph. The curved

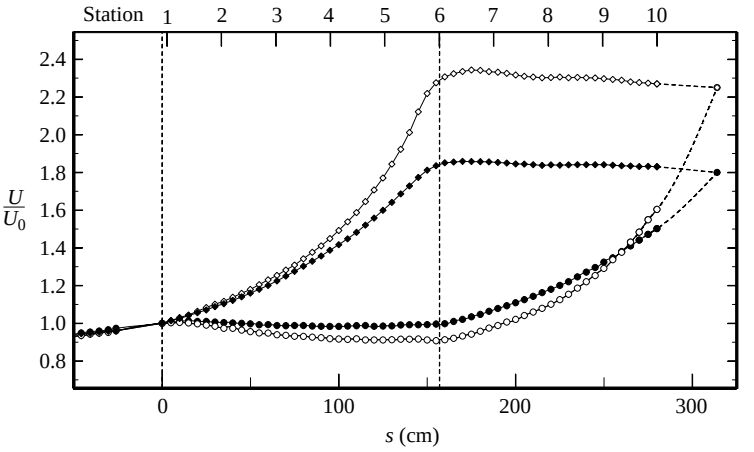

FIGURE 6. Streamwise development of the circumferential component of mean velocity in all four flow configurations. Last point is an extrapolation of measurements to the end of the wind tunnel. Symbols correspond to flows as follows: ●, A_m; ○, A_s; ◆, R_m; ◇, R_s.

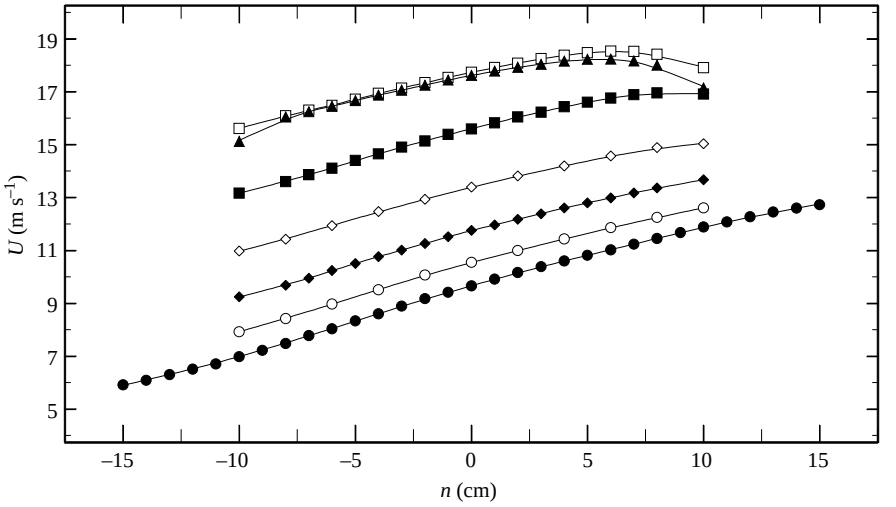

FIGURE 7. Transverse profiles of the circumferential component of mean flow velocity in R_m at measurement stations: ●, 1; ○, 2; ◆, 3; ◇, 4; ■, 5; □, 7; ▲, 9.

test section extends from $s = 0$ to 314 cm. The division between the first and second curved test sections is indicated by vertical dashed line at $s = 157$ cm. For flows A_m and A_s, the flow convergence occurs in the second curved subsection of the curved test section and for flows R_m and R_s the convergence occurs in the first subsection. The zone of measurement in the second subsection is limited by the end-effects of the tunnel and for this reason it appears that greater velocities are reached in the cases R_m and R_s where the convergence occurs in the first subsection. In fact, the velocity rise in cases A_m and A_s are comparable as the extrapolation based on reduced cross-sectional area shows. The gap in the measurements near the end of the straight wind-tunnel section was due to an experimental design that prevented access to this part of the tunnel with the hot-wire anemometer.

The development of the radial and spanwise profiles of the mean circumferential velocity component in flow R_m is shown in figures 7 and 8 and can be regarded as

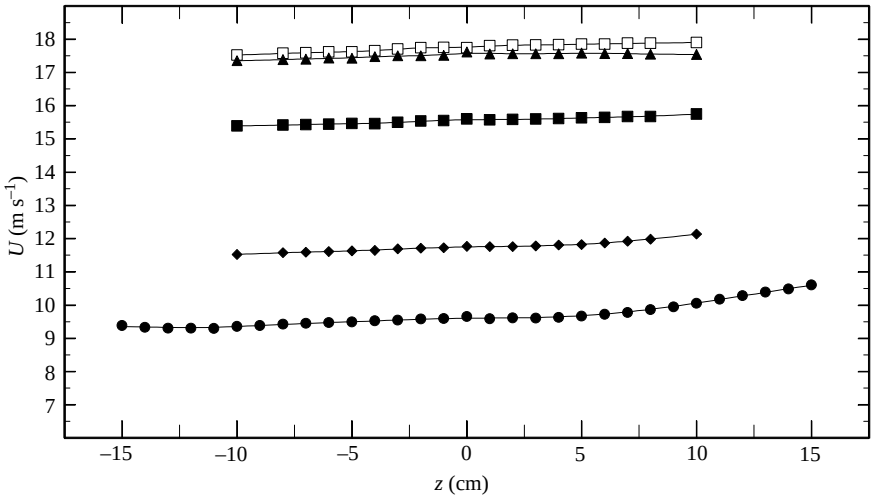

FIGURE 8. Spanwise profiles of the circumferential component of mean flow velocity in R_m at measurement stations: ●, 1; ◆, 5; ■, 7; □, 8; ▲, 9.

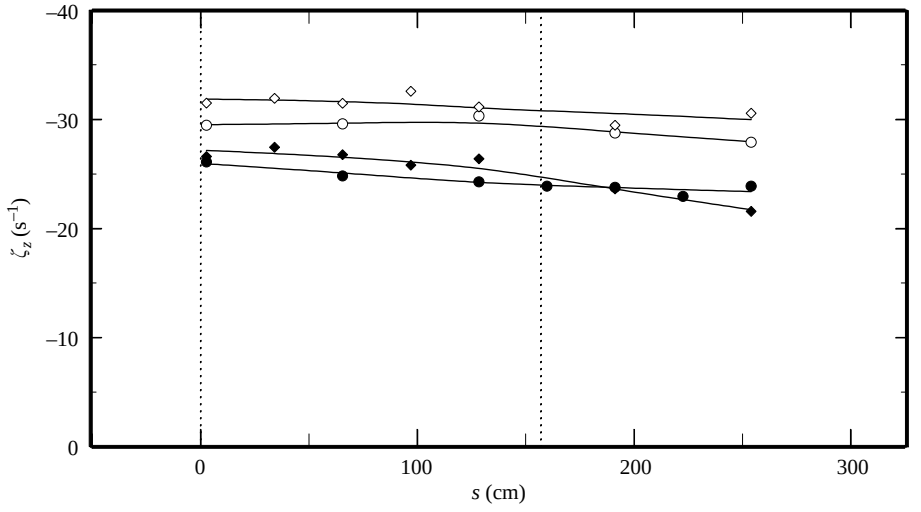

FIGURE 9. Development of the mean flow vorticity, ζ_z, along the wind-tunnel centreline. Dashed lines indicate the beginning of each curved subsection. Symbols as in figure 6.

typical of all four flows. It can be seen that the profiles remain approximately linear near the tunnel centreline ($n = 0$) although curvature and convergence do have an effect on the speed and rate of shear.

The streamwise development of the mean flow vorticity, ζ_z, for each of the four flows is shown in figure 9. The values of ζ_z show some scatter, as we might expect; however, the trend of a gradual loss of vorticity is clear in each case. The greater loss of vorticity in flow R_m can be traced to a loss of mean shear as shown in figure 7. Note that the full expression for vorticity (equation (1)) was used to calculate the values of vorticity from the velocity data.

The development of S and Q (measures of the mean flow curvature and convergence) along the wind-tunnel centreline are shown in figures 10 and 11, respectively. Both have substantial peak values and we would expect strong effects on the

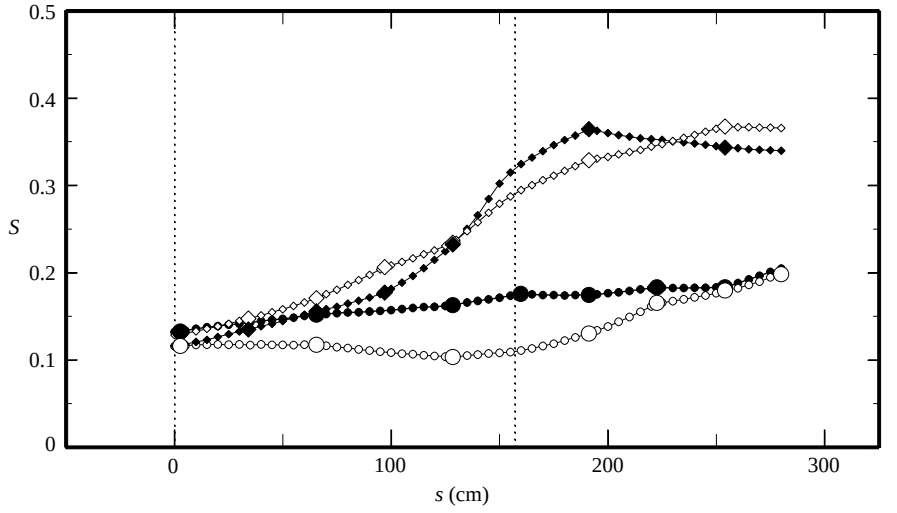

FIGURE 10. Development of the mean curvature parameter, S, along the wind-tunnel centreline. Dashed lines mark the beginning of each curved subsection. Symbols as in figure 6. Mean velocity was measured at all points marked by symbols, whereas the transverse velocity gradient was measured only at the points marked by large symbols.

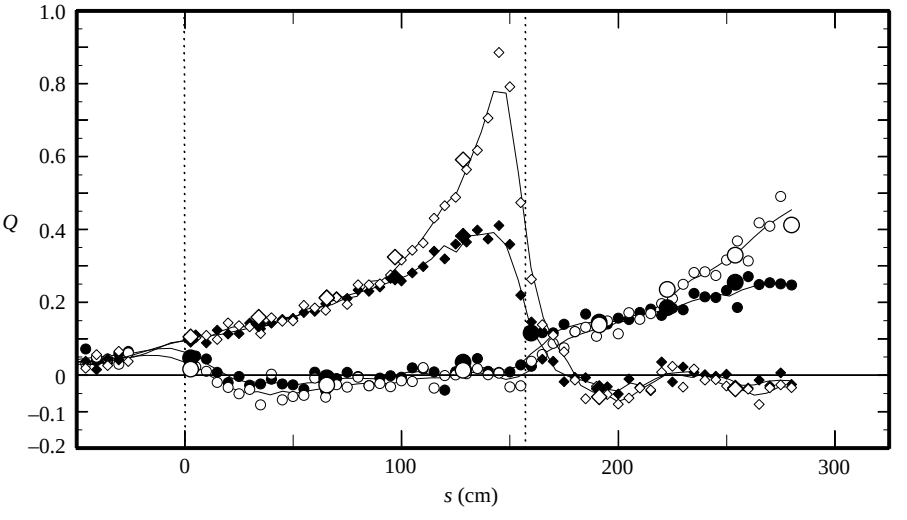

FIGURE 11. Development of the mean acceleration parameter, Q, along the wind-tunnel centreline. Dashed lines mark the beginning of each curved subsection. Symbols as in figure 6. The streamwise mean velocity gradient was based on mean velocity measured at all points marked by symbols, whereas the transverse velocity gradient was measured only at the points marked by large symbols.

turbulence. For the non-converging subsections, S is approximately constant, but, in the converging sections, S rises nearly in proportion to the rise in mean velocity, U. Cases R_m and R_s have higher values of S because of the greater mean velocity achieved there. Q rises throughout the converging sections because of the nonlinear rise in streamwise strain rate that accompanies the linear decrease in cross-sectional area (see § 3.2). In summary, in the subsections without convergence Q is small;

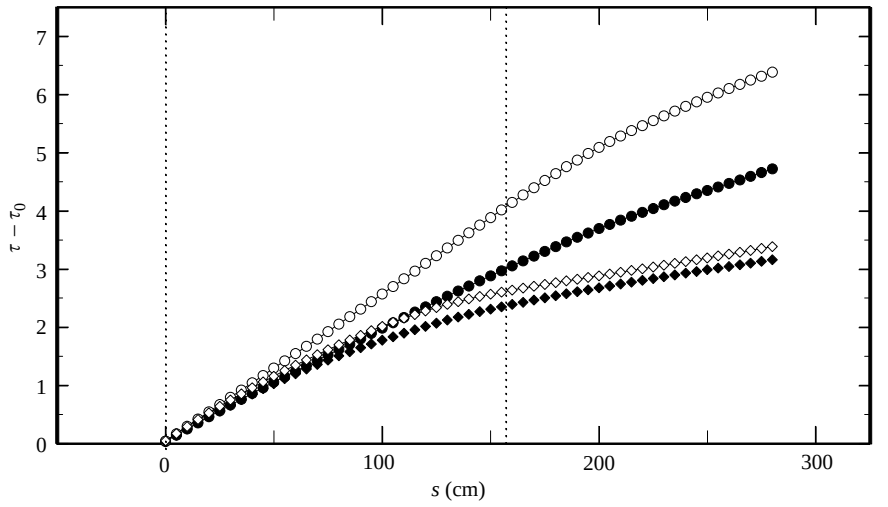

FIGURE 12. Development of the mean shear strain, τ, along the wind-tunnel centreline. Note that shear strain in the straight tunnel prior to the start of curvature, τ_0, is 8.4 units. Symbols as in figure 6.

S is relatively constant, and we would expect the turbulence to adjust towards a fixed structure as observed by HT in their experiments of prolonged constant flow curvature. However, where Q is non-zero, and increasing, we have a rise in S that must be taken into account when assessing the impact of flow convergence on the turbulence structure. Unfortunately, it is not possible to apply flow convergence while keeping S constant if we are to conserve the mean vorticity of the flow.

The accumulated mean shear strain, τ, along the wind-tunnel centreline for each of the flows is shown in figure 12. It can be seen that the greatest shear strain occurs in the flows A_m and A_s, owing to the lower centreline speeds in these flows. The values of $\Delta\tau$ in the first curved (non-converging) subsection of A_m and A_s are 3 and 4, respectively, which is less than the $\Delta\tau = 4.5$ required for full adjustment to flow curvature. In the second curved (converging) subsection, the values of $\Delta\tau$ are less than in the first subsection in both cases owing to the higher centreline speeds. Flow A_s has the greater shear strain of the two because of its higher shear rate. In cases R_m and R_s, the flow convergence occurs in the first curved subsection giving higher speeds throughout and less shear strain than in flows A_m and A_s. The value of $\Delta\tau$ in the second curved subsection of flows R_m and R_s, where the speed is high throughout, is less than 1.

6.3. *Turbulence kinetic energy and length scales*

A comparison of the development of q^2 in each of the four flows is shown in figure 13 on semi-logarithmic scales to allow the comparison of exponents of growth. Prior to the start of flow curvature, q^2 is growing in all four flows at similar rates. In the curved test section all flows showed a decline in q^2; however, the rate of decline depended on the applied streamwise strain rate. In the first curved subsection, the flows subjected to flow convergence, R_m and R_s, show more rapid decay of q^2, with the stronger convergence producing the stronger effect. In the second curved subsection flows A_m and A_s are subjected to flow convergence and show comparable exponents of decay. Similarly, the second curved subsection of flows R_m and R_s, where the flow convergence is removed, show very similar decay rates of q^2 to those in the first curved

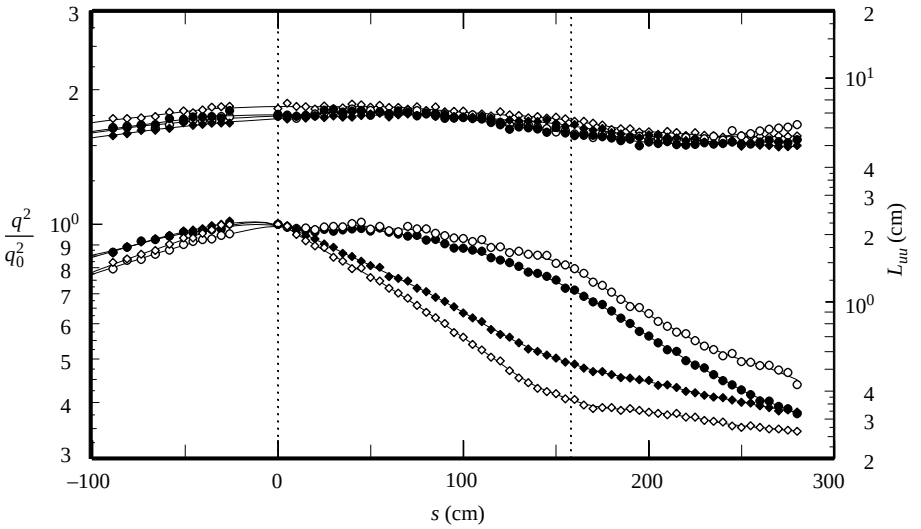

FIGURE 13. Comparison of streamwise development of $q^2 = \overline{u^2} + \overline{v^2} + \overline{w^2}$ and the streamwise integral length scale, L_{uu}, along the wind-tunnel centreline for all flows. Symbols as in figure 6.

subsection of flows A_m and A_s prior the application of flow convergence. Fortuitously perhaps, the q^2 levels from flows R_m and A_m converge in the second subsection and those of R_s and A_s appear to be approaching convergence outside of the range of measurement.

The development of the streamwise integral length scale, L_{uu}, is also shown in figure 13 to indicate generally the size of the turbulent motions (5–7 cm) and to show the effects of curvature and flow convergence on them. L_{uu} was computed using Taylor's frozen flow hypothesis and the temporal integral scale estimated by integration of the autocorrelation to its first zero. In the straight wind-tunnel section, the turbulence is subjected to shearing only and L_{uu} grew at similar rates in all four flows. The application of curvature arrested this growth and produced some modest decay. The similarity of the development of L_{uu} among the four flows in the curved tunnel, each with different flow convergences, leads us to conclude that flow convergence has, at most, a weak effect on the integral length scales of the flow.

6.4. *Reynolds stress anisotropy*

The stress anisotropy provides a quantitative comparison of the structure of the velocity fluctuations that develop under the combined influence of flow curvature and convergence. The development of the anisotropy in the four flows is shown in figures 14–17. In the straight section prior to the start of curvature, the stress anisotropy has a fixed set of values, as described in § 4.1.

The flows A_m and A_s show similar development in the first curved subsection where curvature alone is applied and approach the fixed values reported by HT for prolonged constant curvature of uniform shear flow. In the second curved subsection, the application of flow convergence causes all the normal components: m_{uu}, m_{vv} and m_{ww}, to move towards zero while the shear component m_{uv} is increased in magnitude. The greater rate of convergence in flow A_s produces stronger effects.

At the end of the first curved subsection, the anisotropy components of flows R_m and R_s have similar values to those of A_m and A_s at the end of the second curved subsection where the flow convergence is similar. In the second curved subsection of

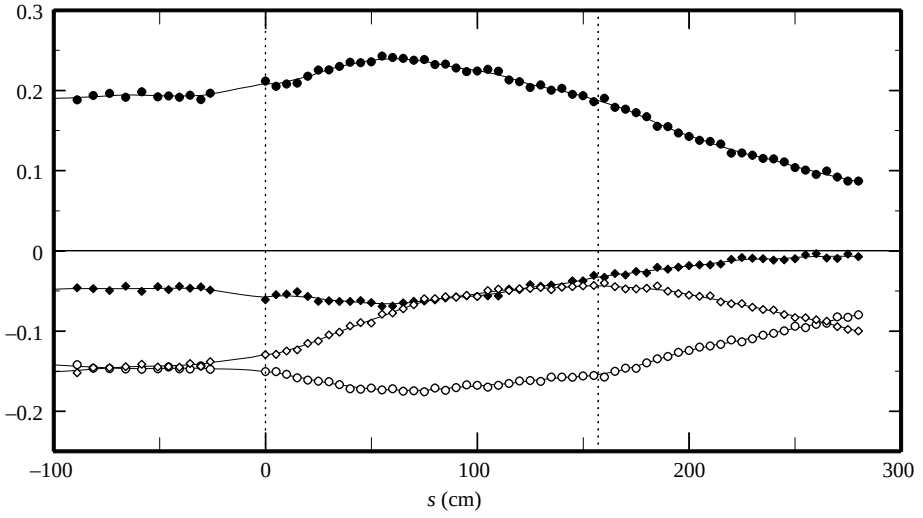

FIGURE 14. Development of the Reynolds stress anisotropy along the wind-tunnel centreline in flow A_m. Dashed lines indicate the beginning of each curved test section. Symbols are as follows: ●, m_{uu}; ○, m_{vv}; ◆, m_{ww}; ◇, m_{uv}.

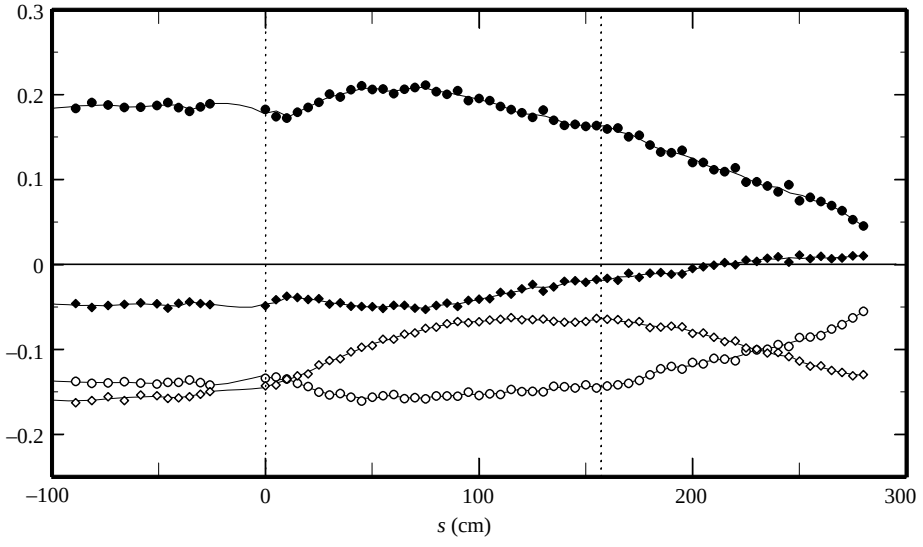

FIGURE 15. Development of the Reynolds stress anisotropy along the wind-tunnel centreline in flow A_s. Dashed lines indicate the beginning of each curved test section. Symbols as in figure 14.

flows R_m and R_s, where the flow convergence is removed and curvature maintained, we see that the anisotropy components recover towards the values expected for curvature acting alone. The sensitivity of the turbulence to convergence is weaker than it is for streamwise flow curvature if we consider the magnitude of the parameters of S and Q shown in figures 10 and 11.

An overall measure of the stress anisotropy is its second invariant, $II = m_{uu}^2 + m_{vv}^2 + m_{ww}^2 + 2m_{uv}^2$. The development of II is shown in figure 18. Comparing the development of II for all four flows shows that application of both curvature and

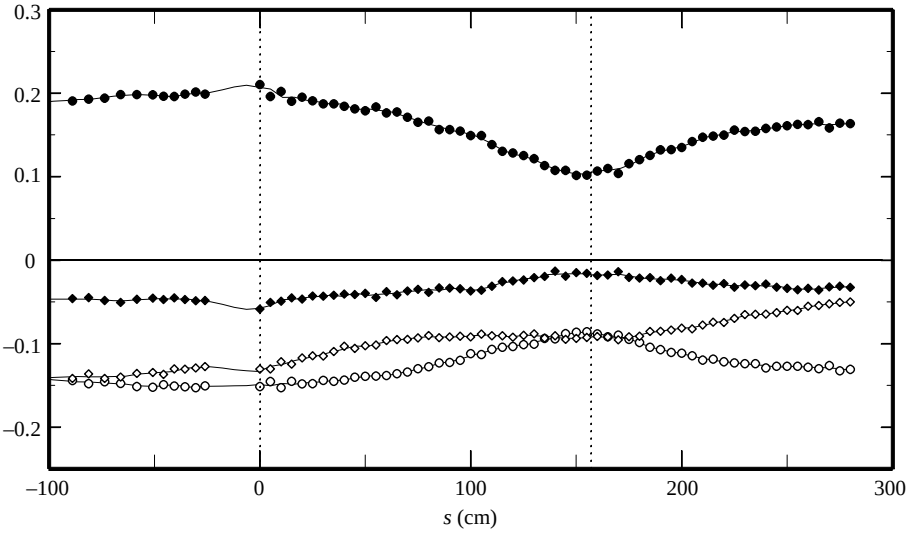

FIGURE 16. Development of the Reynolds stress anisotropy along the wind-tunnel centreline in flow R_m. Dashed lines indicate the beginning of each curved test section. Symbols as in figure 14.

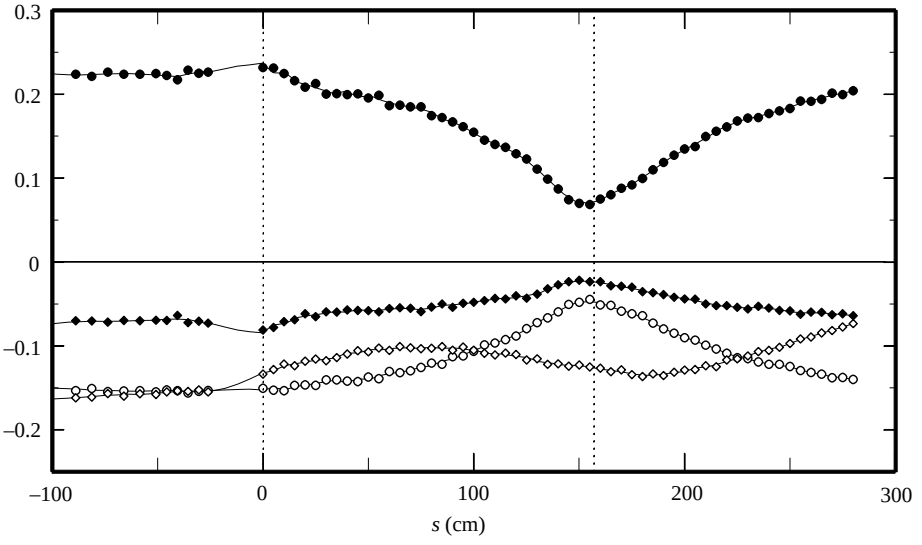

FIGURE 17. Development of the Reynolds stress anisotropy along the wind-tunnel centreline in flow R_s. Dashed lines indicate the beginning of each curved test section. Symbols as in figure 14.

flow convergence causes a reduction of Reynolds stress anisotropy. Removal of the flow convergence allows recovery of the anisotropy.

The development of the Reynolds stresses can be inferred from the development of the components of the stress anisotropy tensor and the development of q^2 shown in figure 13. Some general observations are that the stresses grew in the straight wind-tunnel section with $\overline{u^2} > \overline{w^2} > \overline{v^2} > \overline{uv}$. During the development of the stresses in the curved subsections this order of the stresses is preserved while the stresses

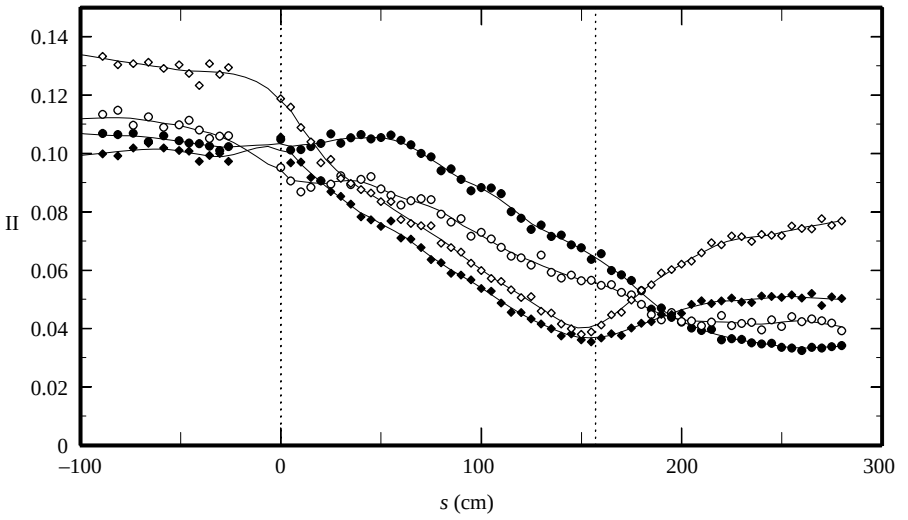

FIGURE 18. Comparison of streamwise development of the second invariant of the Reynolds stress anisotropy tensor, II, along the windtunnel centreline for all flows. Symbols as in figure 6.

generally declined in magnitude. In flows where streamwise strain was applied the shear stress, $\overline{uv}$, was observed to decline the least.

7. Discussion

7.1. *Comparison with curved uniform shear flow experiments*

The experimental study of HT considered the effects of prolonged constant flow curvature on the turbulence of uniform shear flow. One conclusion of the study was that the Reynolds stress anisotropy tended towards fixed values that correlate with the parameter S. These results will be used in comparison to the present results to distinguish the effects of flow convergence on the turbulence structure of the underlying curved flow.

Fitted curves through the equilibrium values of the shear stress anisotropy reported by HT for the range $-0.15 < S < 0.18$ are shown in figure 19. In all of the present experiments, the curvature is applied at the start of the curved test section and maintained through to the end so that in subsections without flow convergence, we would expect that the stress anisotropy would approach the equilibrium curves. Similarly, we could conclude that deviations of the data of the present flows from these curves could be attributed to the flow convergence. This allows us to separate the effects of flow convergence from those of sustained flow curvature.

Flows A_m and A_s have approximately constant values of S prior to the application of flow convergence and, at the end of the first curved subsection, they would be expected to have a structure close to that observed by HT. Values of shear anisotropy at this point are shown on figure 19 as large circles and are close to the equilibrium values. These are starting points for the application of flow convergence and have values of $Q = 0$. The development in the second curved subsection, where flow convergence is applied, is charted as small circles. For flow A_m (solid circles) the value of S remains within a narrow range, while for flow A_s (open circles) the change in S is significant. The effect of applying flow convergence is to direct the trajectory of development above the equilibrium curve of HT.

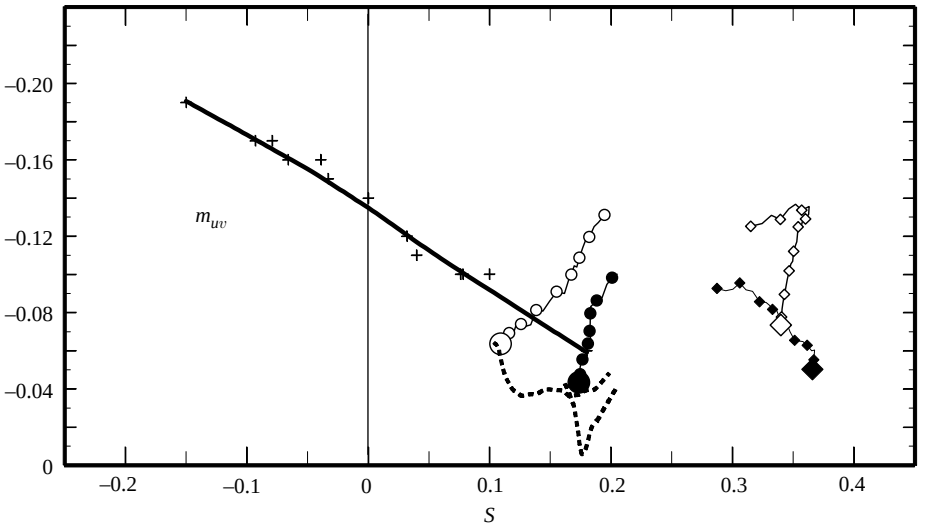

FIGURE 19. Development of the shear component of the Reynolds stress anisotropy from the present flows compared with equilibrium values reported by HT for prolonged constant curvature without acceleration. Solid line and + symbols represent the HT data; ● and ○ represent the development of flows A_m and A_s, respectively, in the second curved subsection during the application of flow convergence; ◆ and ◇ represent the development of the flows R_m and R_s in the second curved subsection after the removal of flow convergence. Dashed lines correspond to the coordinates aligned with maximum shear rate.

The development of shear anisotropy in flows R_m and R_s begins at the end of the first curved subsection with Q equal to 0.4 and 0.9, respectively. In this state, the turbulence is well above the equilibrium data of HT. The relaxation from flow convergence in the second curved subsection ($Q = 0$) is shown as small diamonds that in both cases tend downward towards the equilibrium line of HT. The large diamonds indicate the last measurement point. The initial rise in m_{uv} resulting from removal of flow convergence, most notable in the R_s case, will be discussed in relation to the principal direction of the mean strain rate in the next section.

7.2. *Effect of flow convergence on the principal axes of mean strain and Reynolds stress*

It is clear from the present results that the application of flow convergence to curved shear flow causes a further reduction in the turbulence activity and anisotropy. This reduction in anisotropy is, however, non-uniform with the normal components decreasing and the shear component tending towards values close to those measured in uncurved flow. A partial explanation of this phenomenon can be based on the Reynolds stress equations, (15)–(19) using the explicit appearance of mean strain and turning. More directly, we may consider the relationship between the angle of the principal mean strain rate and principal Reynolds stress anisotropy, θ and γ, to the local streamwise direction. The angle θ was the parameter suggested by Spalart & Shur (1997) as a replacement for S in turbulence modelling of curved flow and the present experimental results provide an excellent opportunity to test their hypothesis in curved and accelerating flow.

Curvature alone does not affect the angle θ which is referred to the curvilinear coordinate system. However, the application of flow convergence causes a turning of the principal mean strain rate towards the streamwise direction and, as described

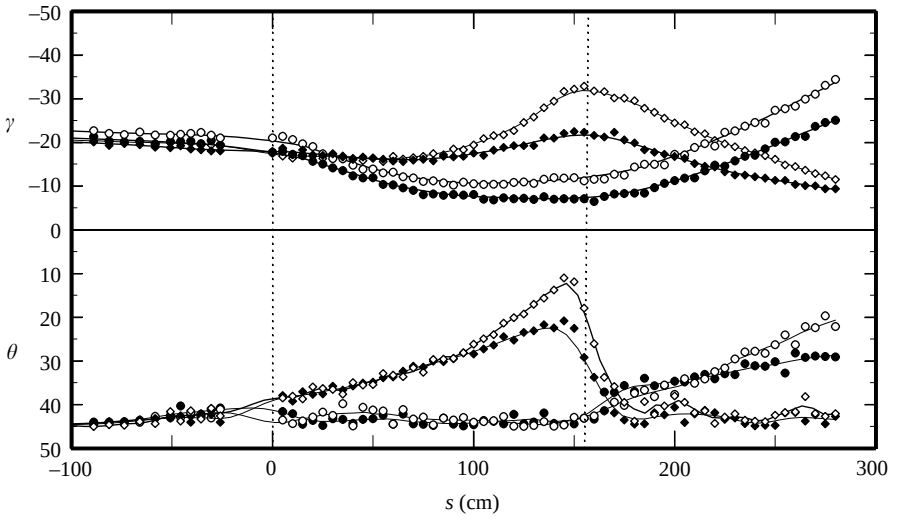

FIGURE 20. Comparison of the streamwise development of the angle of principal mean strain, θ, and the angle of the principal direction of the Reynolds stress anisotropy tensor, γ, measured relative to the streamwise direction. Symbols as in figure 6.

by (10), the rate of turning of this axis is proportional to the rate of change of Q. Figure 20 shows this effect where θ adjusts from 45° (prior to flow convergence) to as little as 10° in flow R_s where Q is greatest. The rate of change of θ is nearly uniform in these cases. In the second curved subsections of R_m and R_s, where flow convergence is removed, θ quickly readjusts to approximately 45°.

Figure 20 shows the response of γ to the application of curvature and streamwise strain rate. Prior to the start of curvature $\gamma = -22°$ and this adjusts to approximately $-10°$ near the end of the first subsection of A_m and A_s under the influence of curvature alone ($\theta = 45°$). The difference $(\theta - \gamma)$ adjusts gradually from 65° at the start of curvature to 55° in these flows. Where flow convergence is applied, θ decreases and figure 20 shows that γ tracks the reduction of θ very closely. In the second curved subsection of flow R_m and R_s, θ suddenly returns to 45° and γ relaxes towards –10°. Throughout the application of flow convergence $(\theta - \gamma) \sim 55°$, as in the cases having curvature alone. Whether the curvature and flow convergence are applied simultaneously or sequentially does not seem to affect this relationship significantly. This turning of the Reynolds stress tensor away from the s-coordinate is partially responsible for the observed changes in the components of the Reynolds stress anisotropy, as may be described by a rotational transformation of coordinates. The shear component in (s, n)-coordinates is particularly sensitive to the angle γ

$$m_{uv} = -\tfrac{1}{2}(m_1 - m_2)\sin(-2\gamma), \tag{20}$$

where m_1 and m_2 are the principal values of the anisotropy.

Summarizing the above observations: the angle between the principal mean strain rate direction and the s-coordinate is reduced by flow convergence, but is unaffected by curvature. The angle between the principal mean strain rate direction and the principal Reynolds stress direction is reduced by positive curvature, but is relatively unaffected by the application of flow convergence. As a consequence, positive curvature tends to rotate the principal stress direction towards the s-coordinate and flow convergence tends to rotate it away from the s-coordinate. The effects tend to offset each other

with the result that the shear stress is nearly unaffected by some combinations of positive curvature and flow convergence as noted by Scharwz *et al.* (2002). We could also interpret the effect of flow convergence as a rotation of the direction of the maximum mean shear through the angle, β, in the clockwise direction. In this view, the turbulence of converging curved shear flows is equivalent to non-converging curved flows when described in axes rotated through the angle β. Carrying this argument further, for fixed values of S and Q in a flow, we would expect that the structure of the turbulence would reach an asymptote and that this would match the equilibrium data of HT when viewed in coordinates aligned with the maximum shear. To test this hypothesis, we will ignore the rate of change of values of S and Q and transform the shear anisotropy data from flows A_m and A_s shown in figure 19 to coordinates of maximum mean shear rate using the local value of β. These transformed data have been added to figure 19 as dashed lines. (Note that for R_m and R_s, $Q=0$ and so no transformation is required.) The transformed data approach the equilibrium data of HT although there is clearly a transient phase, arising from the rate of change of Q and S, that is most pronounced for flows A_s and R_s.

We will now consider the effect of changing Q and its relationship with flow curvature. It was shown in § 3.2 that the application of flow curvature, such as in the first curved subsections of flows A_m and A_s, causes the rotation of the (s, n)-coordinate directions and the mean shear relative to fixed laboratory coordinates at a rate U_c/R_c. A changing rate of streamwise strain rate (but fixed S), according to (10), causes the mean shear to turn relative to the (s, n)-coordinates. As a result, the total rate of turning of the mean shear relative to the laboratory coordinates is, for constant S,

$$\Lambda = U_c\left(\frac{-1}{R_c} + \frac{-(1-S)}{(1-S)^2+4Q^2}\frac{\partial Q}{\partial s}\right). \tag{21}$$

For positive curvature and flow convergence, as in the second subsection of flows A_m and A_s, the curvature of the flow is effectively increased and the effect is initially significant when we consider the values of Q shown in figure 11. This analysis offers the explanation that the observed double dip of m_{uv} for flow A_s shown in figure 19 (dashed line) before it finally rises towards the equilibrium line is due to the increase in slope of $\partial Q/\partial s$ near the midpoint. The opposite effect occurs at the start of the second subsection of flows R_m and R_s, where $\partial Q/\partial s < 0$ and is large enough in magnitude to effectively reverse the sign of the curvature. As a consequence, the data of R_s shown in figure 19 first moves upward and away from the equilibrium line before finally moving towards it.

The above relationship between streamwise strain rate and streamwise curvature would allow the shear anisotropy in (s, n)-coordinates, m_{uv}, in a converging curved shear flow, having parameters S and Q, to be determined from data for a non-converging curved shear flow having the parameter S_{eq}. The complete formulation is as follows

$$S_{eq} = S + \frac{Q\dfrac{\partial S}{\partial \tau_{max}} + (1-S)\dfrac{\partial Q}{\partial \tau_{max}}}{\sqrt{(1-S)^2+4Q^2}}, \tag{22}$$

$$\beta = \tfrac{1}{2}\tan^{-1}\left(\frac{1-S}{2Q}\right) - \frac{\pi}{4}, \tag{23}$$

$$m_{uv} = -\tfrac{1}{2}(m'_{uu} - m'_{vv})\sin(-2\beta) + m'_{uv}\cos(-2\beta), \tag{24}$$

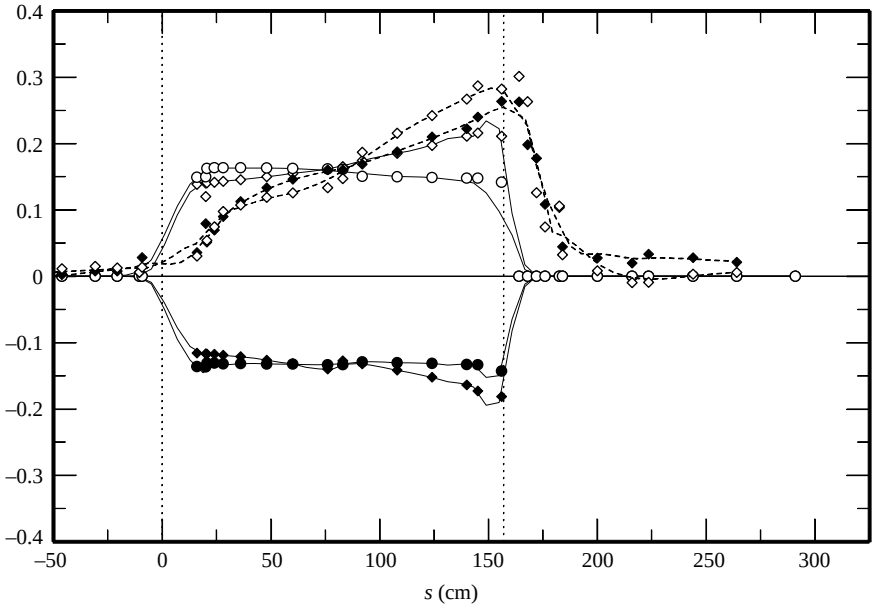

FIGURE 21. Profile of dimensionless curvature and flow convergence parameters, S and Q, in the flow of Akbary (1997). Solid lines joining data points indicate S and dashed lines Q. The circles represent flow without flow convergence ($Q = 0$). The diamonds represent flow which combine flow convergence and curvature.

where m'_{uu}, m'_{vv} and m'_{uv} are the components of anisotropy in the non-converging curved flow and τ_{max} is the total shear strain based on the maximum shear rate; numerically equal to d_1 as given by (8). If S_{eq} is constant then m'_{uu}, m'_{vv} and m'_{uv} would be the asymptotic values measured by HT for prolonged constant curvature. In more general circumstances of changing S_{eq} the state of stress would have to be measured or estimated from a turbulence model. It is worth noting that (22) involves partial second derivatives of the streamwise component of mean velocity that would be very difficult to calculate from experimental data.

7.3. *Comparison to the accelerating, curved uniform shear flow experiments of Akbary* (1997)

The experiments of Akbary (1997) used the same experimental facility as Roach (2001) to study the simultaneous application of flow curvature and convergence to straight uniform shear flow in the first curved subsection (like flows R_m and R_s) and the subsequent removal of flow curvature and convergence in the second curved subsection where the flow was allowed to relax towards uncurved uniform shear flow. There are four flows in total; two with only curvature that may be used as baseline flows, and two with curvature and flow convergence. The profiles of S and Q from the Akbary experiments are shown in figure 21. One of these experiments is unique because it combines negative curvature with flow convergence. The levels of $|S|$ and Q in the first curved subsection are comparable to the first curved subsection of flow R_m in the present experiments.

The response of the shear component of the anisotropy, m_{uv}, is shown in figure 22. There is clearly an increase in m_{uv} resulting from flow acceleration in the first curved subsection and this increase is greater in magnitude for positive S, especially when we consider that the magnitude of S is greater in this case. If the effects of curvature and

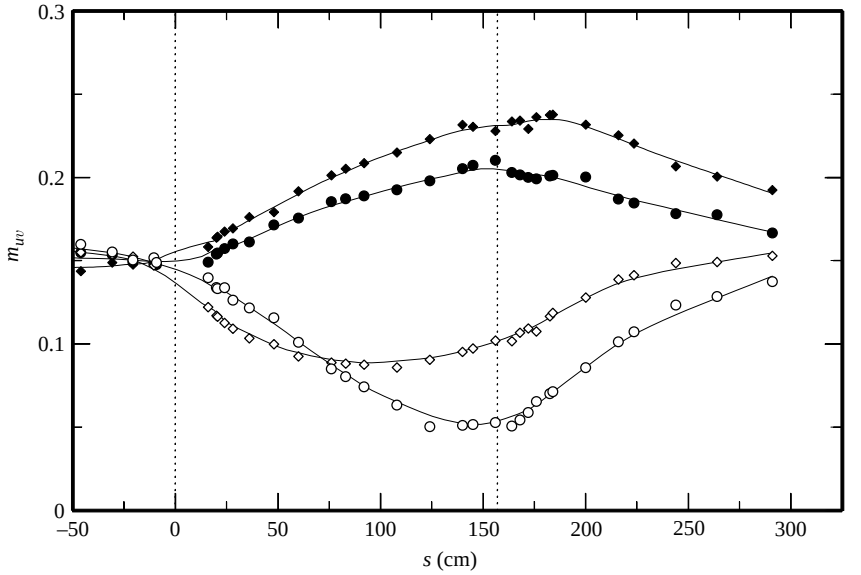

FIGURE 22. Development of the shear component of the stress anisotropy in the four uniform shear flows of Akbary (1997). Symbols correspond to those used in the mean flow description of figure 21.

flow convergence were independent and therefore simply additive, we would expect that the effect of convergence on m_{uv} would not depend on the sign of S. In the second curved subsection, where the flow adjusts to become a straight uniform shear flow, the turbulence relaxes and m_{uv} from the four different flows converge, although within the region of measurement they do not fully recover the values held prior to the start of curvature. The development of q^2 and L_{uu} for these flows is shown in figure 23.

7.4. *Comparison with the accelerating boundary-layer flow*

The similarity between outer-layer turbulence of a boundary layer and that of uniform free shear flow such as those of the present experiments was used by Chebbi *et al.* (1998) to successfully explain some of the effects of convex curvature on the boundary layer. The analogy was based on the equivalence of local mean shear rates and turbulence anisotropy around the mid-thickness of the boundary layer while ignoring flow inhomogeneity. Here, we will extend the analogy to include the effects of favourable pressure gradient with the hope of providing a partial explanation of its observed effects on boundary-layer turbulence. It must be remembered, however, that direct viscous effects are absent from the uniform shear flow and therefore those aspects of pressure gradient effects that scale with viscosity cannot be represented.

Schwarz *et al.* (2002) studied the development of a turbulent boundary layer that was simultaneously subjected to both convex (positive) curvature and pressure gradients. The flow most relevant to the present study is their TS2 flow with $\delta/R \sim 0.05$. It was subjected to zero pressure gradient, case ZPGC, and strong favourable pressure gradient with $10^6(\nu/U_e^2)(\mathrm{d}U_e/\mathrm{d}x) = 1.5$, case SFPGC. As shown in § 3.2, the present flows also have $(1/U_c^2)(\mathrm{d}U_c/\mathrm{d}x) \sim$ constant. The principal angles of the mean strain rate and Reynolds stress at the midpoint of the boundary layer, $y/\delta \sim 0.5$ have been chosen as the basis of comparison between these flows and the present study. For this location, values of S and Q and the principal angle of mean strain rate and Reynolds

$s - s_o$ (cm)	$\tau - \tau_o$	S	Q	θ	γ	$\theta - \gamma$
Flat plate	–	0	0	45	−26	71
0.0	0.0	0.11	0.12	37	−26	63
6.11	0.73	0.12	0.14	36	−24	60
12.2	1.32	0.13	0.17	34	−22	56
18.3	1.62	0.14	0.22	31	−20	51

TABLE 3. Properties of boundary layer flow TS2 with combined strong favourable pressure gradient and curvature (SFPC) from Schwarz *et al.* (2002). Mean flow and turbulence quantities correspond to $y/\delta \sim 0.5$.

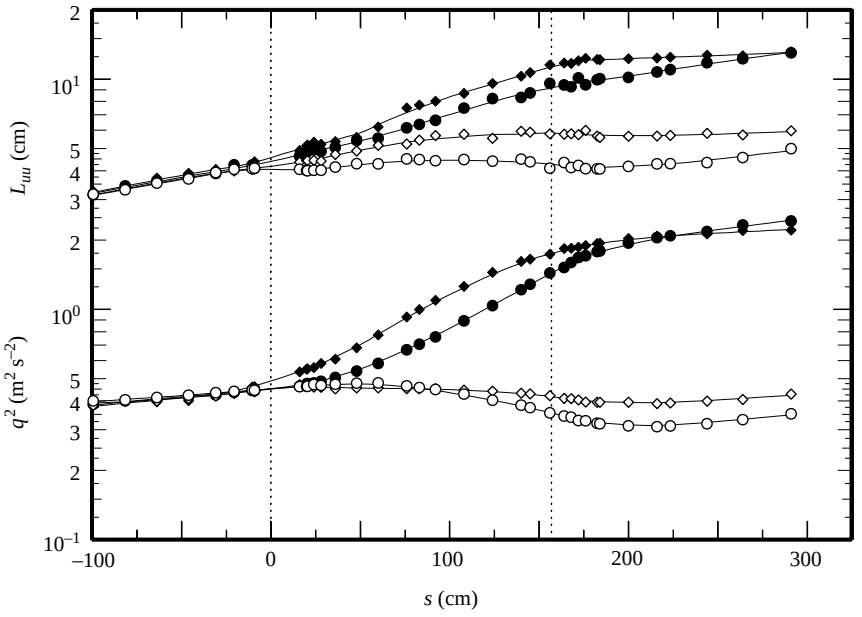

FIGURE 23. Development of the turbulence scales, q^2 and L, in the four uniform shear flows of Akbary (1997). Symbols correspond to those used in the mean flow description of figure 21.

stress for SFPGC are given in table 3 where we have $S \sim 0.12$ and Q ramping up from 0.12 at the start of curvature to 0.22 after 15° of turning or 1.6 units of shear strain. These conditions closely correspond to the first curved subsection of flow R_m in the present study up to the point $s = 75$ cm. In the discussion of the SFPGC case, Schwarz *et al.* (2002) make the qualitative observation that there is practically no adjustment at all to the combined curvature and pressure gradient; a very similar observation to that made for the present flow. According to the present discussion, this results from the cancelling effects of positive curvature and favourable pressure gradient on the direction of the principle direction of the Reynolds stress tensor.

The value given by Schwarz *et al.* (2002) for the principal Reynolds stress direction for a flat-plate boundary layer is $\gamma = -26°$ and presumably this would be taken as a starting point for development where $\theta = 45°$. As the flow develops, the results approach $\theta = 31°$ and $\gamma = -20°$. This gives the angle between the principal mean strain rate and the principal Reynolds stress, $\theta - \gamma \sim 70°$ prior to the application of curvature and pressure gradient and 51° at the last point of measurement. The

s (cm)	Q	θ	γ	$\theta-\gamma$
ZPG*	0	45	−26	71
940	0.11	39	−19	58
990	0.34	27	−42	69

TABLE 4. Properties of boundary-layer flow (uncurved) subjected to strong favourable pressure gradient from Blackwelder & Kovasnay (1972). Mean flow and turbulence quantities correspond to $y/\delta \sim 0.5$. Zero pressure gradient (ZPG) data from flat plate data of Schwarz *et al.* (2002).

corresponding values for flow R_m shows an adjustment from $\theta = 45^\circ$ and $\gamma = -22^\circ$ to $\theta = 32^\circ$ and $\gamma = -16^\circ$. We conclude that the response observed for principal angles of stress and mean strain rate in the present uniformly sheared flow is at least qualitatively similar to this boundary-layer flow.

Another interesting comparison is with the uncurved accelerating boundary layer. In the experiment by Blackwelder & Kovasnay (1972), the value of $10^6(\nu/U_e^2)(\mathrm{d}U_e/\mathrm{d}x)$ started from 0 at $s < 900$ cm and reached a maximum of 1.5 at $s = 1000$ cm. Values of Q and the principal angle of the Reynolds stress were extracted from their published data for $y/\delta \sim 0.5$ and are given in table 4. Similar to the present accelerating flows, the value of θ declined and γ increased with the difference, $60^\circ < \theta - \gamma < 70^\circ$. This, too, agrees with the present conclusion that acceleration has a weak effect on the angle between principle Reynolds stress and mean strain rate.

Warnack & Fernholz (1998) reported a substantial increase in the maximum value of m_{uv} (located at $y^+ \sim 500$) in two of their accelerating boundary layers. Cases 1 and 2 have $10^6(\nu/U_e^2)(\mathrm{d}U_e/\mathrm{d}x) = 2$ and 4 and Reynolds numbers based on the momentum thickness of 2500 and 900, respectively. An evaluation of the mean velocity profile in Case 1 at the point of maximum acceleration ($x = 3.1$ m) gives $Q \sim 0.17$. For Case 2, the mean shear rate in the vicinity of maximum acceleration is weak and at $y^+ \sim 500$ difficult to determine accurately. We could say that $Q > 0.85$ at $x > 1.45$ m. In both Cases 1 and 2, prior to the start of acceleration, $m_{uv} = -0.15$ (typical of sheared turbulence) and this increased to maximum values −0.195 and −0.205 somewhat downstream of the position of maximum acceleration. These observed increases in m_{uv} can be explained using the arguments regarding principal mean strain rate presented above as follows. The acceleration causes the principal direction of mean strain rate, θ, to rotate towards the streamwise direction (as described by (9)) and, according to the present findings, the principal direction of the Reynolds stresses, γ, rotates with it with a fixed angular separation of 65° while retaining fixed invariants. This causes γ to become more negative and, according to (20), this will produce an increase in m_{uv}. In Case 1 with $Q \sim 0.17$, we have $\theta \sim 35^\circ$ and $\gamma \sim -30^\circ$ which gives (assuming m_1 and m_2 in (20) are fixed) $(m_{uv})_{Q=0.17}/(m_{uv})_{Q=0} = 1.34$. Before considering Case 2, it should be noted that the maximum rise in m_{uv} predicted by (9) and (20) is a factor of 1.6 which occurs at $Q = 0.6$. At higher Q, the rise of m_{uv} is less and, at very large Q, it tends to a factor of 1.19. In Case 2, if we take $Q > 0.85$, $\theta < 15^\circ$ and $\gamma < -50^\circ$ we obtain $(m_{uv})_{Q<0.85}/(m_{uv})_{Q=0} < 1.5$. This simple analysis does fit the observed rise in m_{uv} roughly and explains why the two flows may have similar results in spite of the stronger acceleration in Case 2. The rate of change of Q has also been hypothesized (according to (22)) to have an effect on m_{uv}; increasing Q has effects similar to convex curvature and decreasing Q has similar effects to concave

curvature. The rate of change of Q is difficult to evaluate and it is not clear whether the development of m_{uv} presented by Warnack & Fernholz (1998) shows such effects.

8. Conclusion

Uniformly sheared turbulence was subjected to various combinations of stabilizing streamline curvature and flow convergence. These included application of flow convergence to curved flow, and removal of flow convergence from curved flow. The work of Akbary (1997) was also described for the cases of simultaneous application of flow convergence and curvature, stabilizing and destabilizing, and their simultaneous removal. The experiments revealed that the mean streamwise strain rate was the best measure of the effects of flow convergence on curved uniform shear flow and that there exist similarities between the effects of the streamwise strain rate and the strain rate produced by curvature. Both streamwise strain rate and stabilizing curvature reduce the production of turbulence energy and the overall Reynolds stress anisotropy. They have opposite effects, however, on the shear component of the stress anisotropy, m_{uv}. This effect was best explained by consideration of the principal angle of the mean strain rate and Reynolds stress directions. The data showed that stabilizing curvature reduces the angle between these two directions, and hence reduces m_{uv}, while streamwise strain rate does not significantly affect it. Streamwise strain rate does, however, turn the principal mean strain rate towards the streamwise direction and therefore moves the principal direction of the Reynolds stress away from the streamwise direction, increasing m_{uv}. In both cases, the angle between the principal stress and principal mean strain is increased so that turbulence production is reduced.

A relationship between streamwise strain rate and streamwise curvature was formed on the basis of their producing equivalent directions of the principal mean strain rate measured relative to a laboratory frame. It shows that increasing streamwise strain rate effectively increases the flow curvature and a decreasing streamwise strain rate effectively decreases the flow curvature. In one of the flows where flow convergence was suddenly removed, the rate of change of streamwise strain rate was sufficiently negative to effectively create conditions similar to destabilizing curvature for a short distance. The present experimental data were found to be in agreement with these predictions. The influential role of the principal mean strain rate suggested by the present experiments lends credence to the hypothesis of Spalart & Shur (1997) that it is an important parameter for use in turbulence modelling.

A comparison to the accelerating curved boundary-layer study of Schwarz *et al.* (2002), Warnack & Fernholz (1998) and Blackwelder & Kovazny (1972) showed that the effects measured in the present flows are roughly consistent with their outer-layer data. The comparison provides some insight into the problem of superimposed favourable pressure gradients and streamwise curvature in boundary-layer flows.

REFERENCES

AGARD 1998 Test Cases for the Validation of LES in Turbulence and Transition, chap. 3: Homogeneous flows. Advisory Report AR-345.

Akbary, H. 1997 Effects of extra strain rates on uniform shear flow and their relevance to impeller flows. PhD thesis, University of New Brunswick, NB Canada.

Bandyopadhyay, P. R. 1989 Convex curvature concept of viscous drag reduction. *Viscous Drag Reduction in Boundary Layers*. AIAA Series on Progress in Astronautics and Aeronautics (ed. D. M. Bushnell & J. N. Hefner), vol. 123, pp. 285–324.

Bandyopadhyay, P. R. & Ahmed, A. 1993 Turbulent boundary layer subjected to multiple curvatures and pressure gradients. *J. Fluid Mech.* **246**, 503–527.

Baskaran, V., Smits, A. J. & Joubert, P. N. 1987 A turbulent flow over a curved hill. Part 1. Growth of an Internal Boundary Layer. *J. Fluid Mech.* **182**, 47–83.

Baskaran, V., Smits, A. J. & Joubert, P. N. 1991 A turbulent flow over a curved hill. Part 2. Effects of streamline curvature and streamwise pressure gradient. *J. Fluid Mech.* **232**, 377–402.

Blackwelder, R. F. & Kovasnay, L. S. G. 1972 Large-scale motion of a turbulent boundary layer during relaminarization. *J. Fluid Mech.* **53**, 61–83.

Bradshaw, P. 1972 *An Introduction to Turbulence and its Measurement*. Pergamon.

Bradshaw, P. 1973 Effects of streamline curvature on turbulent flow. *NATO AGARDograph* 169.

Bruun, H. H. 1995 *Hot-Wire Anemometry: Principles and Signal Analysis*. Oxford University Press.

Castro, I. P. & Bradshaw, P. 1976 The turbulence structure of a highly curved mixing layer. *J. Fluid Mech*, **73**, 265–304.

Chebbi, B., Holloway, A. G. L. & Tavoularis, S. 1998 The response of sheared turbulence to changes in curvature. *J. Fluid Mech.* **358**, 223–244.

Fernholz, H. H. & Warnack, D. 1998 The effects of a favourable pressure gradient and of the Reynolds number on an incompressible axisymmetric turbulent boundary layer. Part 1. The turbulent boundary layer. *J. Fluid Mech.* **359**, 329–356.

Gillis, J. C. & Johnston, J. P. 1983 Turbulent boundary layer flow and structure on a convex wall and its redevelopment on a flat wall. *J. Fluid Mech.* **135**, 123–153.

Harris, V. G., Graham, J. A. H. & Corrsin, S. 1977 Further experiments on nearly homogeneous turbulent shear flow. *J. Fluid Mech.* **81**, 657–687.

Holloway, A. G. L. & Tavoularis, S. 1992 The effects of curvature on sheared turbulence. *J. Fluid Mech.* **237**, 569–603.

Holloway, A. G. L. & Tavoularis, S. 1998 A geometric explanation of the effects of mild streamline curvature on the turbulence anisotropy. *Phys. Fluids* **10**, 1733–1741.

Holloway, A. G. L. & Roach, D. C. 2001 Modelling effects of flow curvature and frame rotation on sheared turbulence. *Turbulence Shear flow Phenomena 2*, Stockholm, Sweden.

Karnik, U. & Tavoularis, S. 1987 Generation and manipulation of uniform shear with the use of screens. *Exps. Fluids* **5**, 255.

Koyama, H. S. 1981 Turbulent shear flows behind a cylinder and sphere in curved channels. *Proc. 3rd Symp. Turbulent Shear Flows, Davis, USA*, pp. 4.12–4.16.

Koyama, H. S. 1983 Effects of streamline curvature on laminar and turbulent wakes. *Proc. 4th Symp. Turbulent Shear Flows, Karlsruhe, Germany*, pp. 141–155.

Lopes, A. S. & Piomelli, U. 2003 Large eddy simulation of the flow in an S-duct. *AIAA Paper* 2003-0964.

Maxey, M. 1982 Distortion of turbulence in flows with parallel streamlines. *J. Fluid Mech.* **124**, 261–282.

Nakayama, A. 1987 Curvature and pressure gradient effects on a small-defect wake. *J. Fluid Mech.* **175**, 215–246.

Narasimha, R. & Sreenivasan, K. R. 1973 Relaminarization in highly accelerated turbulent boundary layers. *J. Fluid Mech.* **61**, 417–447.

Patel, V. C. & Sotiropoulos, F. 1997 Longitudinal curvature effects in turbulent boundary layers. *Prog. Aerospace Sci.* **33**, 1–70.

Plesniak, M. W., Mehta, R. D. & Johnston, J. P. 1994 Curved two-stream turbulent mixing layers: three-dimensional structure and streamwise evolution. *J. Fluid Mech.* **270**, 1–50.

Ramjee, V. & Neelakandan, D. 1989 Development of wake of a rectangular cylinder in a curved stream. *Exps. Fluids* **7**, 395–399.

Roach, D. C. 2001 Structure of swirling and accelerating turbulent cured shear flows. PhD thesis, University of New Brunswick.

Savill, A. M. 1983 The trubulence structure of a highly curved two-dimensional wake. In *Structure of Complex Turbulent Shear Flow, IUTAM Symp., Marseille* (ed. R. Dumas & L. Fulachier). Springer.

Schwarz, A. C. S., Plesniak, M. W. & Murthy, S. N. B. 2002 Response of turbulent boundary layers to multiple strain rates. *J. Fluid Mech.* **458**, 333–377.

Spalart, P. R. & Shur, M. 1997 On the sensitization of turbulence models to rotation and curvature. *Aerospace Sci. Technol.* **5**, 297–302.

Spalart, P. R. & Watmuff, J. H. 1993 Experimental and numerical study of a turbulent boundary layer with pressure gradients. *J. Fluid Mech.* **249**, 337–371.

Tavoularis, S. & Karnik, U. 1989 Further experiments on the evolution of turbulent stresses and scales in uniformly sheared turbulence. *J. Fluid Mech.* **204**, 457–478.

Warnack, D & Fernholz, H. H. 1998 The effects of a favourable pressure gradient and of the Reynolds number on an incompressible axisymmetric turbulent boundary layer. Part 2. The boundary layer with relaminarization. *J. Fluid Mech.* **359**, 357–381.

Webster, D. R., DeGraaff, D. B. & Eaton, J. K. 1996 Turbulence characteristics of a boundary layer over a two-dimensional bump. *J. Fluid Mech.* **230**, 53–69.

Weygandt, J. H. & Mehta, R. D. 1995 Three-dimensional structure of straight and curved plane wakes. *J. Fluid Mech.* **282**, 279–311.

Wu, X. O. & Squires, K. D. 1998 Numerical investigation of the turbulent boundary layer over a bump. *J. Fluid Mech.* **362**, 229–271.